

https://doi.org/10.3799/dqkx.2019.951



# 中国东北软流圈地幔中的原始橄榄岩质地幔:来自大兴安岭地区新生代玄武岩的地球化学证据

薛笑秋<sup>1</sup>, 陈立辉<sup>1\*</sup>, 刘建强<sup>2</sup>, 何叶<sup>1</sup>, 王小均<sup>1</sup>, 曾罡<sup>1</sup>, 钟源<sup>1</sup>

1. 南京大学地球科学与工程学院, 内生金属矿床成矿机制研究国家重点实验室, 江苏南京 210023

2. 河海大学海洋学院, 海洋地质研究所, 江苏南京 210098

**摘要:** 为了进一步了解中国东北新生代玄武岩地幔源区的物质属性, 报道了大兴安岭哈拉哈河—柴河地区新生代玄武岩的全岩主量、微量元素和 Sr、Nd、Pb、Hf 同位素组成。哈拉哈河—柴河玄武岩属钠质碱性系列, 具有与洋岛玄武岩相似的微量元素特征, 如富集大离子亲石元素 (LILEs)、明显的 Nb、Ta 正异常等。它们具有中等亏损的 Sr-Nd-Hf 同位素组成 ( $^{87}\text{Sr}/^{86}\text{Sr} = 0.7035 \sim 0.7039$ ,  $\epsilon_{\text{Nd}} = 5.21 \sim 6.55$ ,  $\epsilon_{\text{Hf}} = 10.00 \sim 11.25$ ), 接近中国东部新生代玄武岩的亏损端元。这些玄武岩具有中等的放射成因 Pb 同位素组成 ( $^{206}\text{Pb}/^{204}\text{Pb} = 18.37 \sim 18.57$ ,  $^{207}\text{Pb}/^{204}\text{Pb} = 15.52 \sim 15.54$  和  $^{208}\text{Pb}/^{204}\text{Pb} = 38.24 \sim 38.43$ ), 在  $^{206}\text{Pb}/^{204}\text{Pb} - ^{207}\text{Pb}/^{204}\text{Pb}$  相关图上位于 4.42~4.45 Ga 的地球等时线之间。它们在 Sr-Nd-Pb 同位素相关图中均落入地幔柱来源的、高  $^3\text{He}/^4\text{He}$  比 ( $>30R_a$ ) 的洋岛玄武岩范围内, 暗示其源区可能存在来自深部地幔的古老原始地幔物质。此外, 这些玄武岩具有高 MgO (8.49%~11.58%)、高 Ni ( $174 \times 10^{-6} \sim 362 \times 10^{-6}$ ) 和高  $\text{Mg}^\#$  (59.1~66.9) 的特征, 表明它们接近于原始岩浆的成分。反演的哈拉哈河—柴河玄武岩的原始岩浆组成具有中等的  $\text{SiO}_2$ 、低  $\text{Al}_2\text{O}_3$  以及高  $\text{CaO}/\text{Al}_2\text{O}_3$  比的特征, 与石榴子石橄榄岩高压 ( $>2.5$  GPa) 实验熔体的成分相当, 暗示玄武岩的源区岩性最可能为橄榄岩。对以原始地幔 (而不是亏损地幔) 的微量元素为初始成分的饱满石榴子石二辉橄榄岩进行低程度 (1%~2%) 部分熔融的模拟计算, 产生的熔体与哈拉哈河—柴河玄武岩具有一致的微量元素特征, 这进一步支持了上述推断。综上所述, 认为大兴安岭地区哈拉哈河—柴河玄武岩的源区含有来自深部地幔的古老的橄榄岩质原始地幔组分。

**关键词:** 新生代玄武岩; 软流圈; 原始地幔; 地球化学; 中国东北; 岩石学。

中图分类号: P581

文章编号: 1000-2383(2019)04-1143-16

收稿日期: 2018-11-13

## Primordial Peridotitic Mantle Component in Asthenosphere beneath Northeast China: Geochemical Evidence from Cenozoic Basalts of Greater Khingan Range

Xue Xiaoqiu<sup>1</sup>, Chen Lihui<sup>1\*</sup>, Liu Jianqiang<sup>2</sup>, He Ye<sup>1</sup>, Wang Xiaojun<sup>1</sup>, Zeng Gang<sup>1</sup>, Zhong Yuan<sup>1</sup>

1. State Key Laboratory for Mineral Deposits Research, School of Earth Science and Engineering, Nanjing University, Nanjing 210023, China

2. Institute of Marine Geology, College of Oceanography, Hohai University, Nanjing 210098, China

**Abstract:** In order to further explore the nature of mantle source beneath the Northeast China, it presents major, trace element, and Sr-Nd-Pb-Hf isotopic compositions for the Cenozoic intra-plate volcanic rocks from the Halaha-Chaihe field in the Greater Khingan Range. These volcanic rocks are mainly alkaline (sodic) basalts, and generally exhibit OIB-like incompatible trace element characteristics, e.g. enrichment in large lithophile elements (LILEs) and positive Nb-Ta anomalies. They show moderate depleted Sr-Nd-Hf isotopic compositions ( $^{87}\text{Sr}/^{86}\text{Sr} = 0.7035 \sim 0.7039$ ,  $\epsilon_{\text{Nd}} = 5.21 \sim 6.55$ ,  $\epsilon_{\text{Hf}} = 10.00 \sim 11.25$ ) and almost repre-

基金项目: 国家自然科学基金项目 (Nos.41688103, 41672049).

作者简介: 薛笑秋 (1994-), 男, 硕士研究生, 从事火成岩岩石学研究。ORCID: 0000-0003-4601-6342. E-mail: xuexiaoqiu1994@gmail.com

\* 通讯作者: 陈立辉, E-mail: chenlh@nju.edu.cn

引用格式: 薛笑秋, 陈立辉, 刘建强, 等, 2019. 中国东北软流圈地幔中的原始橄榄岩质地幔: 来自大兴安岭地区新生代玄武岩的地球化学证据. 地球科学, 44(4): 1143-1158.

sent the most depleted mantle end-member among the Cenozoic basalts in eastern China. Their Pb isotopic compositions ( $^{206}\text{Pb}/^{204}\text{Pb}=18.37-18.57$ ,  $^{207}\text{Pb}/^{204}\text{Pb}=15.52-15.54$ ,  $^{208}\text{Pb}/^{204}\text{Pb}=38.24-38.43$ ) range between 4.42 Ga and 4.45 Ga geochrons on the  $^{207}\text{Pb}/^{204}\text{Pb}$  versus  $^{206}\text{Pb}/^{204}\text{Pb}$  diagram. They also show similar Sr-Nd-Pb isotopic compositions with those mantle plume-derived ocean island basalts ( $^3\text{He}/^4\text{He}>30 R_a$ ), which implies a deep mantle source. The high MgO (8.49%–11.58%), Ni( $174\times 10^{-6}-362\times 10^{-6}$ ) contents and high Mg<sup>#</sup> values (59.1–66.9) of these basalts imply that their compositions are close to those of the primary magmas. The calculated primitive compositions of Halaha-Chaihe basalts show moderate SiO<sub>2</sub>, low Al<sub>2</sub>O<sub>3</sub> contents and high CaO/Al<sub>2</sub>O<sub>3</sub> ratios, which are accordant with the compositions of experimental melts of garnet peridotite under high pressure (>2.5 GPa) conditions, suggesting a garnet peridotitic mantle source. Moreover, trace-element modeling suggests low-degree melts from a primitive mantle (rather than a depleted mantle) are consistent with these basalts. In summary, it is suggested that the mantle source of the Halaha-Chaihe basalts from the Greater Khingan Range contains ancient, primordial, peridotitic component from the deep mantle.

**Key words:** Cenozoic basalt; asthenosphere; primordial mantle; geochemistry; Northeast China; petrology.

地幔对流可以将深部地幔物质“输送”至浅部地幔,并发生减压熔融形成玄武质熔体.因此通过研究该过程的最终产物——玄武岩的地球化学组成,可以获得深部地幔的相关信息.中国东部的新生代玄武岩是世界上最经典的大陆板内岩浆岩之一,在南起海南岛北抵黑龙江的广大区域内,断续分布了大量以玄武岩为主的火山岩,出露面积达 8 万 km<sup>2</sup> (陈霞玉等,2014).在中国东部新生代玄武岩的早期研究中,虽然对其岩石成因持不同观点,但是普遍认为玄武岩源区岩性是来自软流圈的地幔橄榄岩 (Zhou and Armstrong,1982;刘若新,1992).

随着实验岩石学的进展以及近年来非传统稳定同位素在玄武岩研究中的应用,不同学者从中国东部新生代玄武岩的源区中识别出了辉石岩、榴辉岩和碳酸盐组分等 (Tang *et al.*,2007; Chen *et al.*,2009; Zhang *et al.*,2009,2011,2016; Zeng *et al.*,2010,2011,2017; Wang *et al.*,2011; 陈立辉等,2012; Xu *et al.*,2012; Yang *et al.*,2012; Hong *et al.*,2013; Li *et al.*,2015,2016; Liu *et al.*,2015,2017;徐义刚等,2018),并且认为这些组分对中国东部新生代玄武岩组成的贡献非常普遍,而这些组分比橄榄岩更加难熔 (Huang *et al.*,2015; Li *et al.*,2016,2017; Liu *et al.*,2016; Yang *et al.*,2016).目前,中国东部新生代玄武岩并非来自单纯的橄榄岩部分熔融这一观点已被广泛接受.基于学界近年来的研究成果,徐义刚等 (2018) 通过总结提出中国东部新生代玄武岩可大致解释为高硅和低硅端元熔体的混合,其中高硅熔体源区为石榴石辉石岩,而低硅熔体源区为含碳酸盐的榴辉岩和橄榄岩.由此可见,由单纯的地幔橄榄岩直接发生部分熔融产生的熔体所形成的玄武岩在中国东部新生代玄武岩中反而缺乏明确的例证.

中国东部新生代玄武岩在微量元素和同位素组成上具有较宽的变化范围,可以用来探讨地幔的不均一性 (Zou *et al.*,2000; Chen *et al.*,2009; Yang *et al.*,2016; Xu *et al.*,2017).这些玄武岩的同位素组成主要呈现出两个趋势:东北和华北地区的玄武岩近似是亏损端元 DMM (Depleted MORB Mantle) 和 EM1 (Enriched Mantle, type 1) 的混合;华南则是 DMM 和 EM2 (Enriched Mantle, type 2) 两端元混合的产物 (图 1).前人的大量研究多关注于两个富集端元 EM1 或 EM2 的地幔源区和物质组成 (Zou *et al.*,2000; Chen *et al.*,2009; Kuritani *et al.*,2009,2011; Zeng *et al.*,2011; 陈立辉等,2012; Chu *et al.*,2013; Kuritani *et al.*,2013; Li *et al.*,2015; Sun *et al.*,2015,2016; Zhang *et al.*,2016; Zhang and Guo,2016; Wang *et al.*,2017; Yu *et al.*,2018),而通常认为这个共同的亏损端元更可能代表来自软流圈地幔的橄榄岩组分 (Zou *et al.*,2000; 陈立辉等,2012; 赵勇伟和樊祺诚,2012; Ho *et al.*,2013; Zhang *et al.*,2016; Zhang and Guo,2016; Chen *et al.*,2017; Meng *et al.*,2018; 徐义刚等,2018).大兴安岭地区哈拉哈河—柴河玄武岩的同位素组成恰好位于这个亏损端元的位置 (图 1).因此,如果要进一步探索中国东部是否存在新生代玄武岩直接来源于单纯的橄榄岩熔融这个问题,哈拉哈河—柴河玄武岩是理想的研究对象.关于哈拉哈河—柴河玄武岩的源区物质属性问题,目前尚存争议:Chen *et al.* (2017) 基于单斜辉石斑晶氧同位素和水含量的研究认为玄武岩源区是再循环辉长质下洋壳、热液蚀变的上洋壳+沉积物和地幔橄榄岩的混合物;而 Ho *et al.* (2013)、赵勇伟和樊祺诚 (2012) 以及 Meng *et al.* (2018) 基于全岩地球化学研究认为玄武岩源区是来自软流圈地幔的石榴子

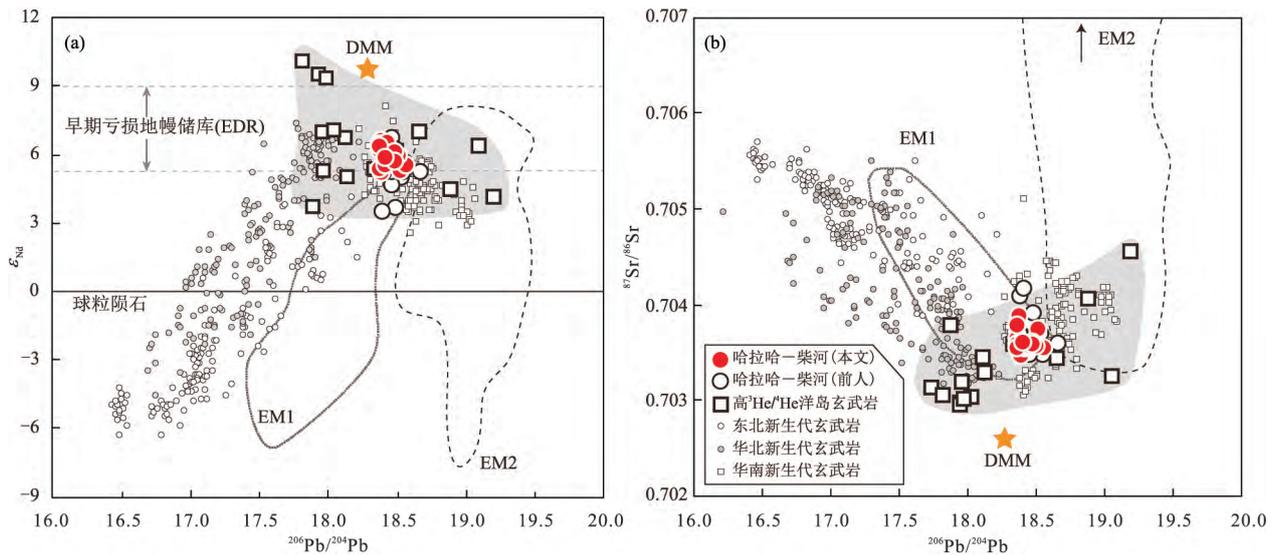


图1 中国东部新生代玄武岩与高 $^3\text{He}/^4\text{He}$ 比值洋岛玄武岩 Sr-Nd-Pb 同位素协变图: (a)  $\epsilon_{\text{Nd}} - ^{206}\text{Pb}/^{204}\text{Pb}$  协变图; (b)  $^{87}\text{Sr}/^{86}\text{Sr} - ^{206}\text{Pb}/^{204}\text{Pb}$  协变图

Fig.1 Variation diagrams of (a)  $\epsilon_{\text{Nd}}$  versus  $^{206}\text{Pb}/^{204}\text{Pb}$  and (b)  $^{87}\text{Sr}/^{86}\text{Sr}$  versus  $^{206}\text{Pb}/^{204}\text{Pb}$  of Cenozoic basalts from eastern China and high  $^3\text{He}/^4\text{He}$  ocean island basalts

亏损地幔(DMM)数据引自 Workman and Hart (2005);早期亏损地幔储库(EDR)数据引自 Boyet and Carlson (2005);高 $^3\text{He}/^4\text{He}$ 比值洋岛玄武岩( $^3\text{He}/^4\text{He} > 30 R_a$  样品的平均值)数据包括巴芬岛(Jackson *et al.*, 2010)、西格陵兰(Graham *et al.*, 1998)、夏威夷(Kurz *et al.*, 1982)、加拉帕戈斯(Saal *et al.*, 2007)、萨摩亚(Jackson *et al.*, 2007)、冰岛(Hilton *et al.*, 1999; Starkey *et al.*, 2009; Stuart *et al.*, 2003)和留尼汪群岛(Graham *et al.*, 1990);中国东部新生代玄武岩数据来源范围较广,略;EM1、EM2型样品数据引自 <http://georem.mpch-mainz.gwdg.de/georoc/>

石二辉橄榄岩,可能直接来源于单纯的橄榄岩熔融。

本文在前人研究的基础上,开展了对哈拉哈河—柴河玄武岩的全岩主量元素、微量元素和 Sr-Nd-Pb-Hf 同位素地球化学联合研究,计算了这些玄武岩的原始岩浆组成,并将其与高温高压实验熔体对比,定量模拟了原始岩浆部分熔融过程中的微量元素组成,深入探讨了这些玄武岩的地幔源区岩性组成和地球化学属性,揭示了玄武岩源区古老的橄榄岩质地幔的存在。

## 1 地质背景和样品描述

哈拉哈河—柴河玄武岩主要出露于兴安地块中南段的哈拉哈河—柴河流域,远离活动大陆边缘,属于典型的大陆板内玄武岩(樊祺诚等, 2008; 赵勇伟等, 2008; 赵勇伟和樊祺诚, 2011, 2012)。在大地构造位置上,研究区所在的兴蒙造山带(Xing'an-Mongolia Orogenic Belt, XMOB)位于古生代中亚造山带的东段,形成于北侧西伯利亚克拉通和南侧华北克拉通之间的汇聚事件(Jahn *et al.*, 2000; Xiao *et al.*, 2015);从地球物理角度上看,研究区位于

大兴安岭—太行山重力梯度带(Daxing'anling-Taihangshan Gravity Lineament, DTGL)北端(图 2a),该梯度带两侧存在布格重力异常的明显差别,不仅将我国东北和华北地区划分为东西两部分,亦形成了地形变化梯度带和岩石圈厚度梯度带(Xu, 2007)。大兴安岭地区的地壳和岩石圈厚度较大,莫霍面深度达 42 km(Tao *et al.*, 2014),岩石圈厚度可达 120~140 km(Zhang *et al.*, 2014)。在中国东部,地震层析成像表明俯冲的太平洋板块滞留在地幔过渡带深度(Huang and Zhao, 2006; Wei *et al.*, 2012),影响范围向西可达  $120^\circ\text{E}$ ,其前缘在地表的投影大致与大兴安岭—太行山重力梯度带一致。

哈拉哈河—柴河火山岩区总体呈北东向分布(图 2b),约 46 座火山主要分布于阿尔山哈拉哈河、扎兰屯绰尔河、柴河和德勒河一带,火山岩分布面积逾  $400\text{ km}^2$ (赵勇伟等, 2008)。结合 K-Ar 法地质测年数据和火山地质特征,研究区火山活动不早于早更新世( $\sim 2.3\text{ Ma}$ ),主要活动期为中更新世和全新世(樊祺诚等, 2011)。

本文共采集哈拉哈河—柴河火山岩样品 33 块,主要分布在该火山区的东西两侧,未对中心地带(德

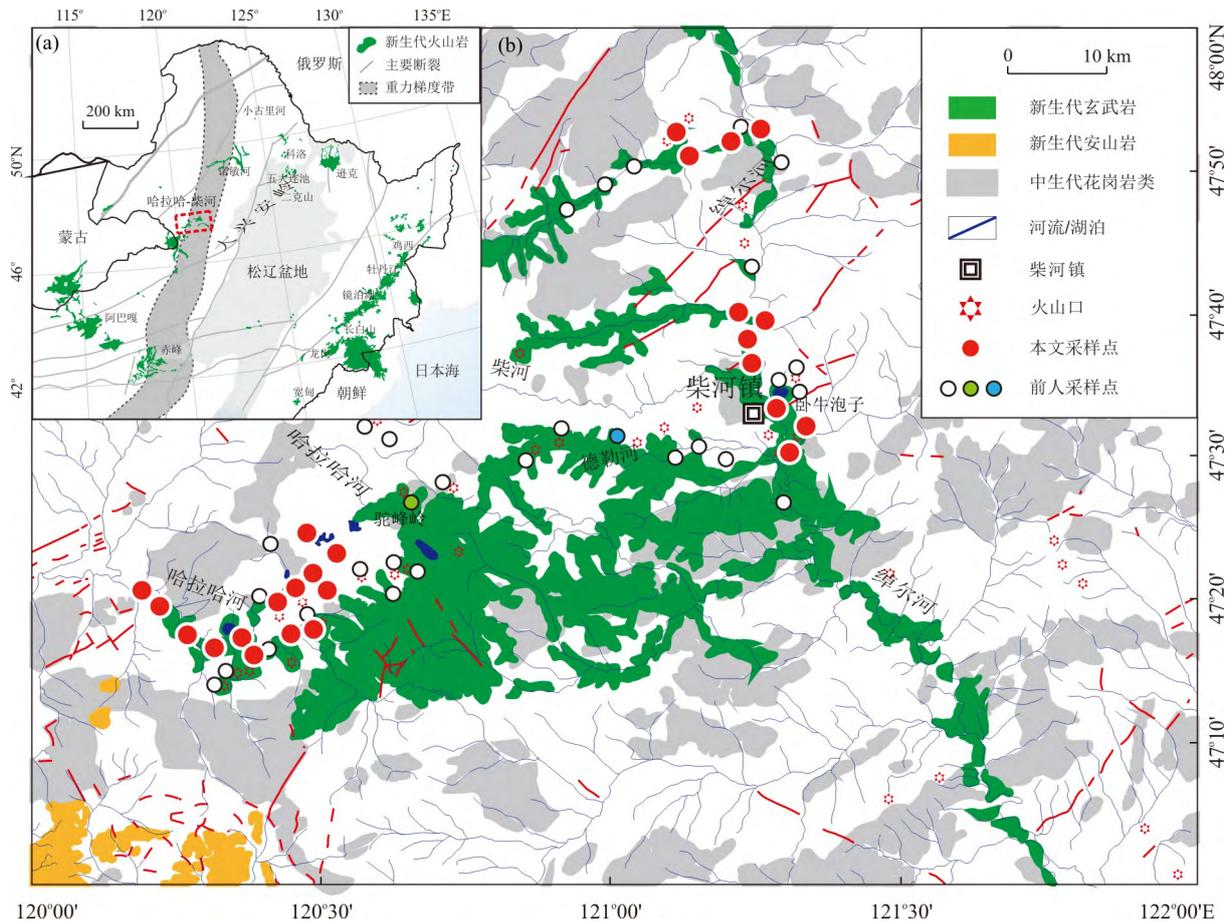


图 2 (a)中国东北地区新生代火山岩分布图;(b)哈拉哈河—柴河玄武岩分布及采样位置

Fig.2 Distribution of Cenozoic volcanic rocks in Northeast China (a) and Late Cenozoic basalts and sample locations in Halaha-Chaihe basalts (b)

图 a 据 Xu (2007); 图 b 据 Ho *et al.* (2013), 灰色虚线区域指示大兴安岭—太行重力梯度带

勒河—驼峰岭一带)进行采样,具体采样位置见图 2b.呈灰黑色—黑色,斑状结构,致密块状构造.斑晶主要为橄榄石,较自形,偶有蚀蚀现象.基质为填间结构和间隐结构,主要由条状斜长石、细粒橄榄石、粒状磁铁矿等钛铁氧化物和隐晶质组成.部分样品中含地幔橄榄岩捕虏体以及橄榄石捕虏晶.考虑到地表风化蚀变等因素会对玄武岩的化学组成造成影响,哈拉哈河—柴河玄武岩样品均取自块状熔岩,并尽量选取新鲜、无风化蚀变的岩石样品用于全岩地球化学分析.

## 2 分析方法

### 2.1 全岩主量元素及微量元素

玄武岩的主量元素分析在南京大学内生金属矿床成矿机制研究国家重点实验室配置的 ARL 9900 (Thermo Scientific)型 X 射线荧光光谱仪上完成的.用

分析天平分别称取烘干后的粉末样品 0.5 g 和助熔剂 (四硼酸锂,  $\text{Li}_2\text{B}_4\text{O}_7$ ) 5 g 混合后倒入铂金坩埚,放入 THEOXD 全自动电熔炉中加热熔融制备玻璃片.另外,用分析天平称取 0.5 g 样品粉末在  $1050^\circ\text{C}$  恒温下进行烧失量 (LOI, loss on ignition) 分析.根据岩石标准参考物质 (BHVO-2 和 GSR-1 和 GSR-3) 的测定值,除了  $\text{P}_2\text{O}_5$  含量的相对误差小于 10% 之外,其他主量元素含量的相对误差均小于 1%.

微量元素分析在西北大学大陆动力学国家重点实验室完成.测试所用的仪器为 ELAN 6100DRC 型电感耦合等离子体质谱仪 (ICP-MS).样品处理过程如下:称取约 50 mg 全岩粉末样品于 Teflon 溶样罐中,加入浓 HF 与浓  $\text{HNO}_3$  的混合酸在  $140^\circ\text{C}$  条件下消解样品并蒸干;继续加入 3 mL  $\text{HNO}_3$ ,再次蒸干;接着加入 3 mL  $\text{HNO}_3$ ,置于  $140^\circ\text{C}$  烘箱中加热约 12 h;最后,冷却样品并转移溶液至容量瓶中,稀释定容到 80 mL.溶样和仪器测试整个流程中采用

BHVO-2、BCR-2 和 AGV-2 三个 USGS 国际岩石标准参考物质进行监控,同时做空白样监控实验室的本底。Li、Sc、V、Cr、Co、Ni、Cu、Zn、Rb、Sr、Y、Zr、Nb、Ta、Ba、Th、U、Hf、Ge 和 REE(稀土元素)的分析精度优于 5%,Cs 和 Pb 的分析精度优于 10%。

## 2.2 全岩 Sr-Nd-Pb-Hf 同位素

样品的全岩 Sr、Nd、Pb、Hf 同位素测试在南京大学内生金属成矿机制研究国家重点实验室完成。样品的 Sr 同位素组成使用 TIMS 进行测定,而 Nd、Pb、Hf 同位素组成则使用 Neptune plus 的 MC-ICP-MS 进行测试。

对 Sr、Nd 同位素而言,化学流程如下:称取样品 200 mg 于 Teflon 溶样罐中,淋滤后加入浓 HF 和浓 HNO<sub>3</sub> 各 1.5 mL 消解样品,置于 130 °C 电热板上加热 48 h。待样品消解后蒸干,重复 3 次加 1 mL 浓 HCl 并蒸干的步骤,最后用 1 mL 4 mol/L 的 HCl 溶解样品转移至离心管。离心后,取上层清液于阳离子交换树脂(Bio-Rad AG50W-X8)进行 Sr、Nd 的化学分离和纯化。具体的化学分离流程参考濮巍等(2005)。对 Pb 同位素而言,化学流程如下:称取样品 200 mg 于 Teflon 溶样罐中,淋滤后加入 2 mL 浓 HF 和 1 mL 浓 HNO<sub>3</sub> 消解样品,置于 130 °C 电热板上加热 48 h。待样品消解后蒸干,加入 1 mL 浓 HNO<sub>3</sub> 再蒸干,然后将样品溶解于 HBr-HNO<sub>3</sub> 的混合酸中转移至离心管。取上层清液于阴离子交换柱(Bio-Rad AG1-X8)进行 Pb 的化学纯化。具体的化学分离步骤参考 Kuritani and Nakamura(2002)。对 Hf 同位素而言,化学流程如下:称取样品 150 mg 于 Teflon 溶样罐中,加入 0.2 mL HClO<sub>4</sub> 浸湿后加入 1 mL 浓 HNO<sub>3</sub> 和 2 mL 浓 HF,于 130 °C 电热板上加热 5 d。待样品完全消解后蒸干,重复 3 次加入 1 mL 6 mol/L HCl 溶解样品并蒸干的步骤。最后加入 5 mL 3 mol/L HCl,置于 80 °C 的电热板上加热 12 h,冷却后转移至离心管。取离心后的上层清液于填充 Eichrom Ln-Spec 树脂的交换柱中进行 Hf 的化学纯化。详细的化学纯化过程见 Yang *et al.*(2010)。

上机测试时,Sr、Nd、Hf 同位素组成分别采用  $^{86}\text{Sr}/^{88}\text{Sr} = 0.1194$ 、 $^{146}\text{Nd}/^{144}\text{Nd} = 0.7219$ 、 $^{179}\text{Hf}/^{177}\text{Hf} = 0.7325$  进行质量分馏校正。Pb 同位素则采取在样品溶液中加入 Tl 元素的方法校正质量分馏。实验过程中使用 USGS 国际岩石标准参考物质对整个化学和测试流程进行了监控,获得 BCR-2 和 BHVO-2 的放射成因同位素组成与前人推荐的参考值基本一致。

## 3 结果分析

### 3.1 全岩主量和微量元素组成

哈拉哈河—柴河玄武岩的主量元素分析结果及相关参数列于附表 1。本文样品属于碱性玄武岩(图 3a),Na<sub>2</sub>O/K<sub>2</sub>O 比大于 1(1.84~2.64),属于钠质玄武岩。哈拉哈河—柴河玄武岩 SiO<sub>2</sub> 含量为 46.7%~50.5%;具有较高的 MgO(8.49%~11.58%)、K<sub>2</sub>O+Na<sub>2</sub>O(4.01%~5.36%)、TiO<sub>2</sub>(1.92%~2.31%),中等的 Al<sub>2</sub>O<sub>3</sub>(12.42%~13.45%)和较低的 P<sub>2</sub>O<sub>5</sub>(0.33%~0.49%)含量(附表 1)。在 Harker 图解上,SiO<sub>2</sub> 与 CaO/Al<sub>2</sub>O<sub>3</sub>、MgO 有负相关关系(图 3)。

哈拉哈河—柴河玄武岩的微量元素分析结果列于附表 2(表中 BHVO-2 微量元素参考值据 Jochum *et al.*(2016))。在球粒陨石标准化的稀土元素配分模式图中(图 4),本文所有样品的配分曲线一致,均向右倾。哈拉哈河—柴河玄武岩的  $\sum\text{REE}$  为  $102.8 \times 10^{-6} \sim 130.1 \times 10^{-6}$ ,  $(\text{La}/\text{Yb})_{\text{N}}$  介于 8.40~11.83,轻、重稀土元素分馏程度较低,未观察到明显的稀土元素异常。但在前人研究中发现个别地区的样品明显偏离了大多数样品:位于驼峰岭火山锥和卧牛泡子附近的样品具有较高的  $\sum\text{REE}$  ( $165.7 \times 10^{-6} \sim 214.5 \times 10^{-6}$ ) 和  $(\text{La}/\text{Yb})_{\text{N}}$  (14.8~17.0),稀土元素配分曲线较陡。而位于研究区中部德勒河流域的样品具有较低的  $\sum\text{REE}$  ( $56.1 \times 10^{-6} \sim 99.5 \times 10^{-6}$ ) 和  $(\text{La}/\text{Yb})_{\text{N}}$  (4.88~6.16),稀土元素配分曲线平缓,并且存在明显的 Eu 正异常(图 4)。

在不相容元素的原始地幔标准化图中(图 5),本文样品的配分曲线基本一致,富集大离子亲石元素(LILEs),Nb、Ta 呈强烈正异常,Pb 表现为负异常或者无异常,Sr 呈弱正异常,Zr、Hf 和 Ti 表现为轻微的负异常或无异常,总体上表现为与洋岛玄武岩(OIB)相似的微量元素特征。这些样品的微量元素配分曲线与内蒙古阿巴嘎新生代碱性玄武岩样品的配分曲线相似,与东北地区新生代钾质玄武岩区别明显,后者更富集强不相容元素,轻、重稀土元素之间的分馏更明显(图 5)。

### 3.2 全岩 Sr、Nd、Pb、Hf 同位素特征

哈拉哈河—柴河玄武岩的 Sr、Nd、Pb、Hf 同位素组成列于附表 3。这些玄武岩具有相对均一的 Sr、Nd、Pb、Hf 同位素组成。其 Sr、Nd、Hf 同位素组成 ( $^{87}\text{Sr}/^{86}\text{Sr} = 0.7035 \sim 0.7039$ ,  $\epsilon_{\text{Nd}} = 5.21 \sim 6.55$ ,  $\epsilon_{\text{Hf}} = 10.0 \sim 11.3$ ) 虽然比 OIB 中的富集端元(EM1

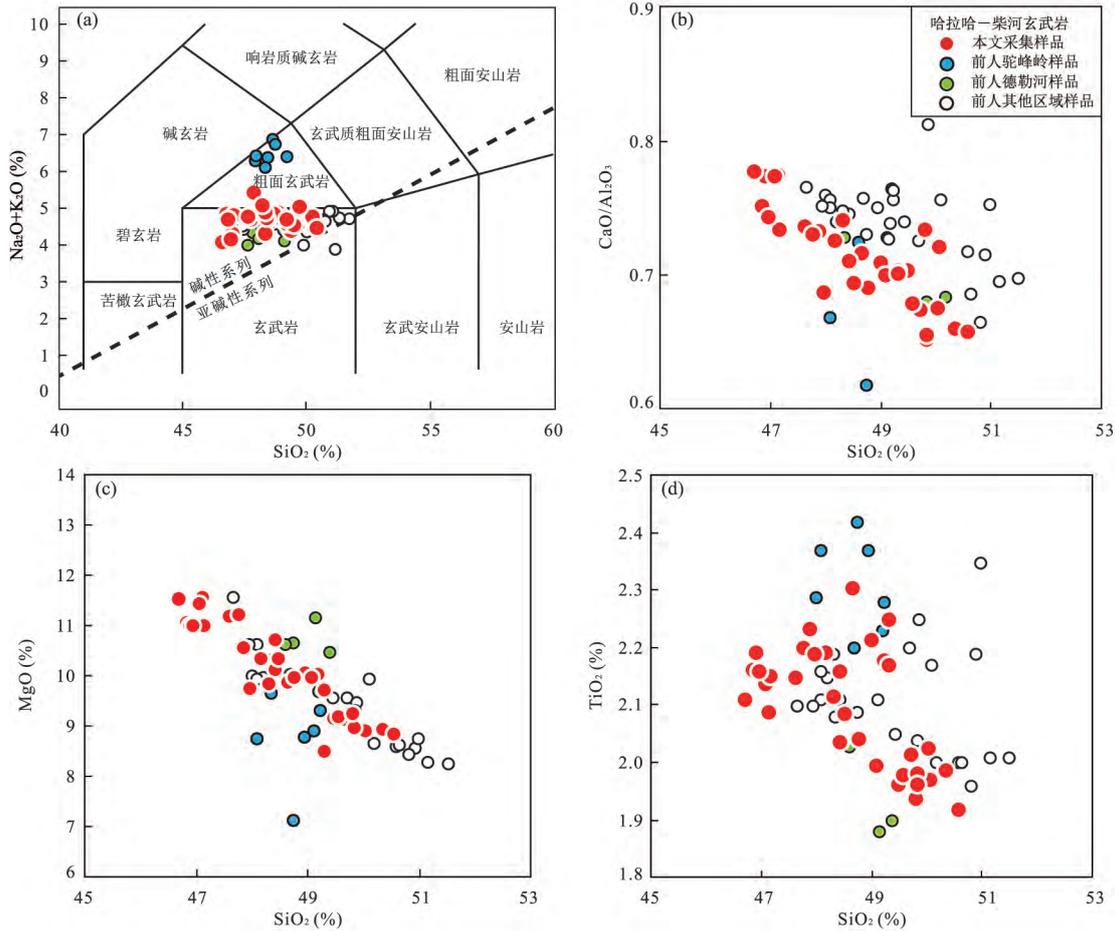


图 3 哈拉哈河—柴河玄武岩 TAS 图 (a),  $\text{SiO}_2 - (\text{CaO}/\text{Al}_2\text{O}_3)$  (b),  $\text{SiO}_2 - \text{MgO}$  (c) 和  $\text{SiO}_2 - \text{TiO}_2$  (d) 相关图解

Fig.3 Total alkali versus  $\text{SiO}_2$  (a); variation of  $\text{CaO}/\text{Al}_2\text{O}_3$ ,  $\text{MgO}$  and  $\text{TiO}_2$  versus  $\text{SiO}_2$  (b–d) for Halaha-Chaihe basalts

图 a 据 Le Bas *et al.* (1986). 红色实心圆代表本次研究哈拉哈河—柴河玄武岩数据; 空心圆、蓝心圆 (驼峰岭) 和绿色圆 (德勒河) 代表前人数据, 引自 Chen *et al.* (2017), Ho *et al.* (2013), Li *et al.* (2017) 以及赵勇伟和樊祺诚 (2012)

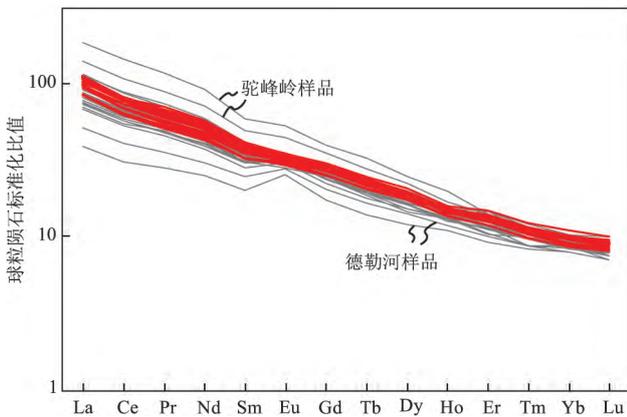


图 4 哈拉哈河—柴河玄武岩球粒陨石标准化稀土元素配分模式图

Fig. 4 Chondrite-normalized REE patterns for Halaha-Chaihe basalts

球粒陨石数据引自 Anders and Grevesse (1989); 红线代表本文数据; 灰线代表前人数据, 引自 Li *et al.* (2017)

和 EM2) 要亏损, 但比绝大多数洋中脊玄武岩富集, 处于 EM1 和 EM2 型玄武岩的交汇区域 (图 1)。本文样品的 Pb 同位素组成均一, 变化范围十分有限 ( $^{206}\text{Pb}/^{204}\text{Pb} = 18.4 \sim 18.6$ ,  $^{207}\text{Pb}/^{204}\text{Pb} = 15.5 \sim 15.6$ ,  $^{208}\text{Pb}/^{204}\text{Pb} = 38.2 \sim 38.4$ )。在  $^{207}\text{Pb}/^{204}\text{Pb} - ^{206}\text{Pb}/^{204}\text{Pb}$  和  $^{208}\text{Pb}/^{204}\text{Pb} - ^{206}\text{Pb}/^{204}\text{Pb}$  相关图上, 哈拉哈河—柴河玄武岩落入印度洋洋中脊玄武岩范围内 (图 6c, 6d)。即在一定的  $^{206}\text{Pb}/^{204}\text{Pb}$  比值情况下, 哈拉哈河—柴河玄武岩具有偏高的  $^{207}\text{Pb}/^{204}\text{Pb}$  和  $^{208}\text{Pb}/^{204}\text{Pb}$  比值, 从而明显区别于太平洋洋中脊玄武岩。值得注意的是, 该地区样品具有相对华北和东北地区新生代玄武岩高的  $\epsilon_{\text{Nd}}$  和  $^{206}\text{Pb}/^{204}\text{Pb}$  比值以及低的  $^{87}\text{Sr}/^{86}\text{Sr}$  比值, 落入华南地区的新生代玄武岩 Sr-Nd-Pb 同位素组成范围内, 靠近中国东部新生代玄武岩的亏损端元 (图 1)。

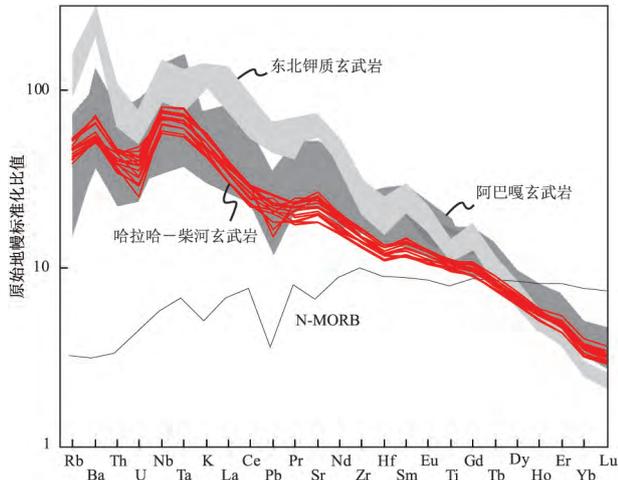


图 5 哈拉哈河-柴河玄武岩的不相容微量元素原始地幔标准化图

Fig.5 Primitive mantle-normalized incompatible trace element patterns for Halaha-Chaihe basalts

原始地幔数据引自 McDonough and Sun(1995), N-MORB 数据引自 Gale *et al.*(2013), 东北钾质玄武岩数据引自 Liu *et al.*(2017), 内蒙古阿巴嘎数据引自 Ho *et al.*(2008)和 Zhang and Guo(2016)

## 4 讨论

### 4.1 分离结晶和地壳混染对玄武岩化学组成的影响

随着 MgO 含量的降低,哈拉哈河-柴河玄武岩的 Ni、Cr、Co 等相容元素含量也逐渐降低(图 7a~7c),指示了橄榄石的分离结晶.而样品 MgO 含量基本都高于 9%,且 MgO 与 TiO<sub>2</sub>、Fe<sub>2</sub>O<sub>3</sub><sup>T</sup> 和 CaO/Al<sub>2</sub>O<sub>3</sub> 比值基本无相关性,暗示岩浆未经历单斜辉石、铁氧化物和钛铁氧化物的分离结晶,其组成与原始岩浆成分接近.另外,在不相容元素原始地幔标准化图上,该区玄武岩并未呈现 Eu 和 Sr 的负异常(图 4,图 5),表明其未经历斜长石的分离结晶.这一系列观察表明,哈拉哈河-柴河玄武岩只经历了橄榄石的分离结晶.而哈拉哈河-柴河玄武岩样品较高的 Mg<sup>#</sup> (59.1~66.9),同样指示它们接近原生岩浆的特点(Fan and Hooper, 1991).

玄武质岩浆在上升过程中还可能受到地壳物质

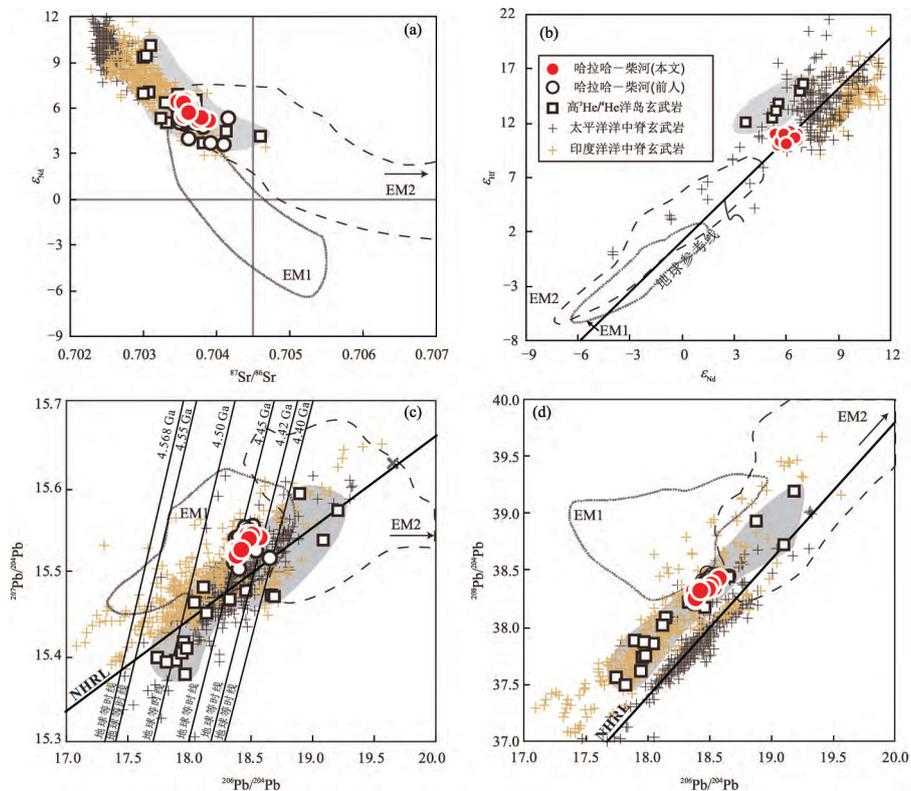


图 6 哈拉哈河-柴河玄武岩 Sr-Nd-Pb-Hf 同位素组成:(a)  $\epsilon_{Nd}$  -  $^{87}Sr/^{86}Sr$  比值协变图;(b)  $\epsilon_{Hf}$  -  $\epsilon_{Nd}$  协变图;(c)  $^{207}Pb/^{204}Pb$  -  $^{206}Pb/^{204}Pb$  比值协变图;(d)  $^{208}Pb/^{204}Pb$  -  $^{206}Pb/^{204}Pb$  比值协变图

Fig.6 Variation diagrams of (a)  $\epsilon_{Nd}$  versus  $^{87}Sr/^{86}Sr$ ; (b)  $\epsilon_{Hf}$  versus  $\epsilon_{Nd}$ ; (c)  $^{207}Pb/^{204}Pb$  versus  $^{206}Pb/^{204}Pb$  and (d)  $^{208}Pb/^{204}Pb$  versus  $^{206}Pb/^{204}Pb$  for the Halaha-Chaihe basalts

Nd-Hf 同位素地球参考线,据 Vervoort *et al.*(2011); NHRL.Pb 同位素北半球参考线,据 Hart (1984); Pb 同位素地球等时线,据 Holmes (1946);高<sup>3</sup>He/<sup>4</sup>He 比洋岛玄武岩数据同图 1, Nd 同位素组成仅包含巴芬岛样品数据;太平洋型和印度洋型 MORB 样品来自 Stracke (2012) 汇总的大洋玄武岩数据

的混染作用,而该过程会改变玄武岩的地球化学组成.哈拉哈河—柴河玄武岩的部分样品在  $\text{SiO}_2$  与  $^{87}\text{Sr}/^{86}\text{Sr}$  协变图上呈现出正相关关系,反映它们受到地壳混染作用的改造(图 7d).但对于大多数样品,尽管  $\text{SiO}_2$  含量变化较大 ( $\text{SiO}_2 = 46.7\% \sim 50.5\%$ ),但 Sr 同位素基本保持不变 ( $^{87}\text{Sr}/^{86}\text{Sr} = 0.7035 \sim 0.7039$ )(图 7d),指示这些样品未经历显著的地壳混染作用.这部分样品反映源区特征的微量元素比值,如 Nb/U 比值(40.7~71.2)均一旦较高,基本符合或高于洋岛玄武岩的平均 Nb/U 比值( $47 \pm 7$ )(Hofmann *et al.*, 1986; Hofmann, 1997),明显高于大陆地壳平均值( $\sim 6.2$ )(Rudnick and Gao, 2003),也说明哈拉哈河—柴河玄武岩大部分样品并未受到地壳物质混染作用的显著影响.此外,野外调研发现,研究区玄武岩中常见地幔捕虏体(赵勇伟和樊祺诚, 2011),指示岩浆的上升速度非常迅

速,因而缺少与周围地壳物质相互作用的时间.

#### 4.2 地幔源区的岩性

近年来,随着实验岩石学的发展,通过玄武岩原始岩浆的化学成分来判别玄武岩地幔源区的岩性成为可能.然而,有关哈拉哈河—柴河玄武岩源区母岩的岩性尚存在争议.赵勇伟和樊祺诚(2012)、Ho *et al.*(2013)和 Meng *et al.*(2018)均通过模拟计算哈拉哈河—柴河新生代玄武岩原始岩浆发生批式部分熔融过程中关键微量元素比值(Sm/Yb、Ce/Yb、La/Yb)的变化,认为源区岩性是来自软流圈地幔的石榴子石二辉橄榄岩;而 Chen *et al.*(2017)则根据单斜辉石斑晶的氧同位素组成和全岩  $\text{H}_2\text{O}/\text{Ce}$ 、Ba/Th 比值变化等特征认为地幔源区受到俯冲古太平洋滞留板片重循环物质持续加入的影响,源区岩性是辉石岩(包括蚀变上洋壳、沉积物和辉长岩质下洋壳)和橄榄岩的混合.

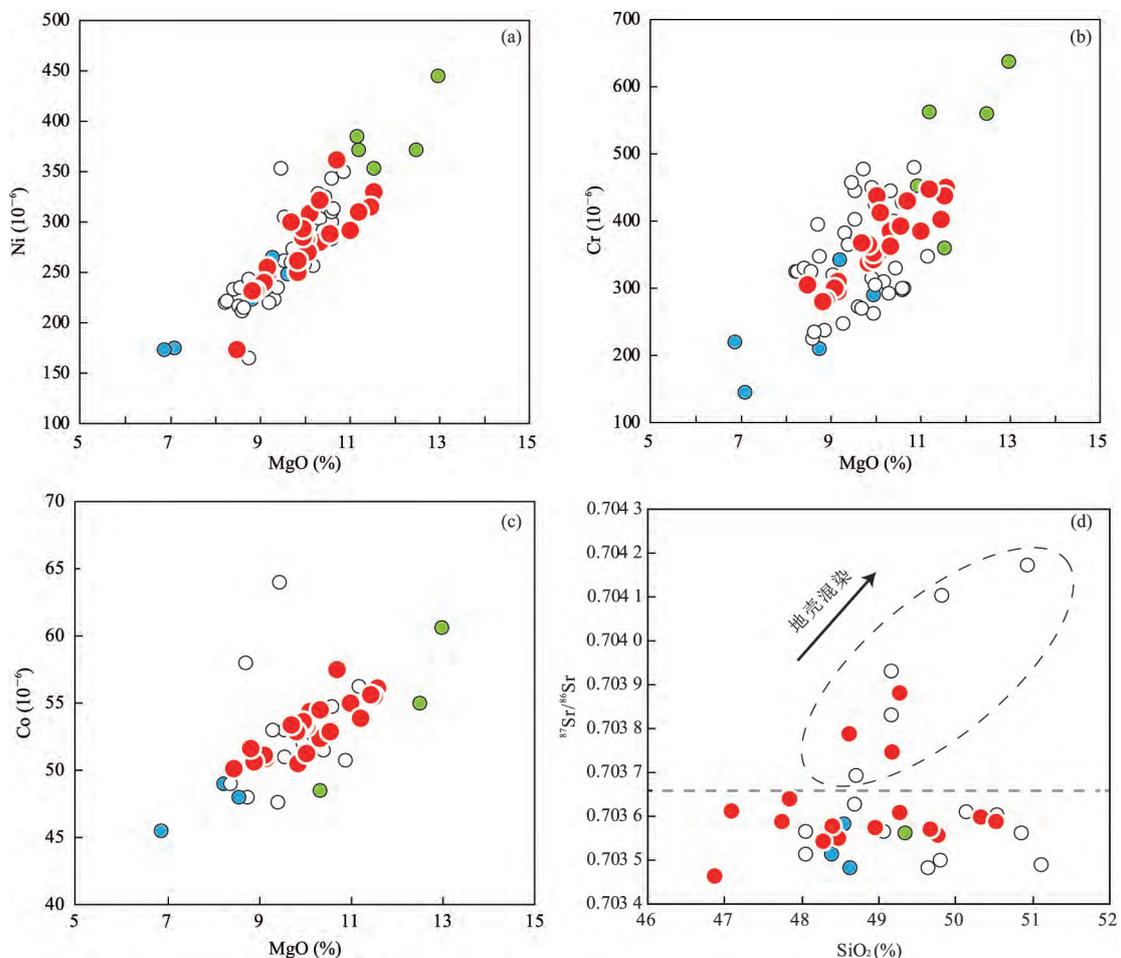


图 7 哈拉哈河—柴河玄武岩 MgO—Ni, Cr, Co 协变图(a~c); Sr 同位素— $\text{SiO}_2$  协变图(d)

Fig.7 Variation diagrams of MgO versus Ni, Cr and Co (a~c) and  $^{87}\text{Sr}/^{86}\text{Sr}$  versus  $\text{SiO}_2$  (d) for the Halaha-Chaihe basalts. 红色实心圆代表本文数据;空心圆、蓝心圆(驼峰岭)和绿色圆(德勒河)代表前人数据,引自 Chen *et al.*(2017)、Ho *et al.*(2013)、Li *et al.*(2017)以及赵勇伟和樊祺诚(2012)

为了进一步限定哈拉哈河—柴河玄武岩的源区母岩岩性,本研究将玄武岩的原始岩浆成分与各种地幔岩石高压实验熔体进行对比.考虑到研究区玄武岩主要只经历过橄榄石的分离结晶,通过逐步增加 0.1%平衡橄榄石(假定  $Fe^{3+}$  占 10%,且  $(Fe^{2+}/Mg)_{olivine}/(Fe^{2+}/Mg)_{melt} = 0.3$ ),据 Roeder and Emslie(1970)的方法将样品主量元素反算到  $Fo_{88}$  时的成分,即可近似代表原始岩浆的主量元素组成(图 8).首先,哈拉哈河—柴河玄武岩具有较高的  $MgO$  含量和较低的  $TiO_2$  含量,明显不同于高压 ( $>2$  GPa)下的富硅辉石岩熔体,而落在贫硅辉石岩和橄榄岩熔体的重叠区域(图 8a).其次,与贫硅辉石岩部分熔融形成的熔体相比,哈拉哈河—柴河玄武岩具有较低的  $Al_2O_3$  和偏高的  $SiO_2$  含量,在保

持较高  $CaO$  含量的同时具有高的  $CaO/Al_2O_3$  比值,更接近橄榄岩发生部分熔融产生的熔体(图 8b~8d).最后,由于沉积碳酸盐具有比地幔显著偏轻的镁同位素组成 ( $\delta^{26}Mg = -5.57\text{‰} \sim -0.38\text{‰}$ ) (Wombacher *et al.*, 2011; Saenger and Wang, 2014; Geske *et al.*, 2015),如果岩浆源区存在再循环的碳酸盐组分,那么玄武岩的镁同位素组成也将是偏轻的.但 Li *et al.* (2017)对哈拉哈河—柴河新生代玄武岩的镁同位素研究 ( $\delta^{26}Mg = -0.29\text{‰} \pm 0.08\text{‰}$ )发现其基本落入正常地幔值范围内 ( $\delta^{26}Mg = -0.25\text{‰} \pm 0.07\text{‰}$ ) (Teng *et al.*, 2010),不支持其源区普遍含有再循环的碳酸盐(驼峰岭样品除外).此外,如果源岩岩性是碳酸盐化橄榄岩或辉石岩,那么它们发生部分熔融产生实验熔

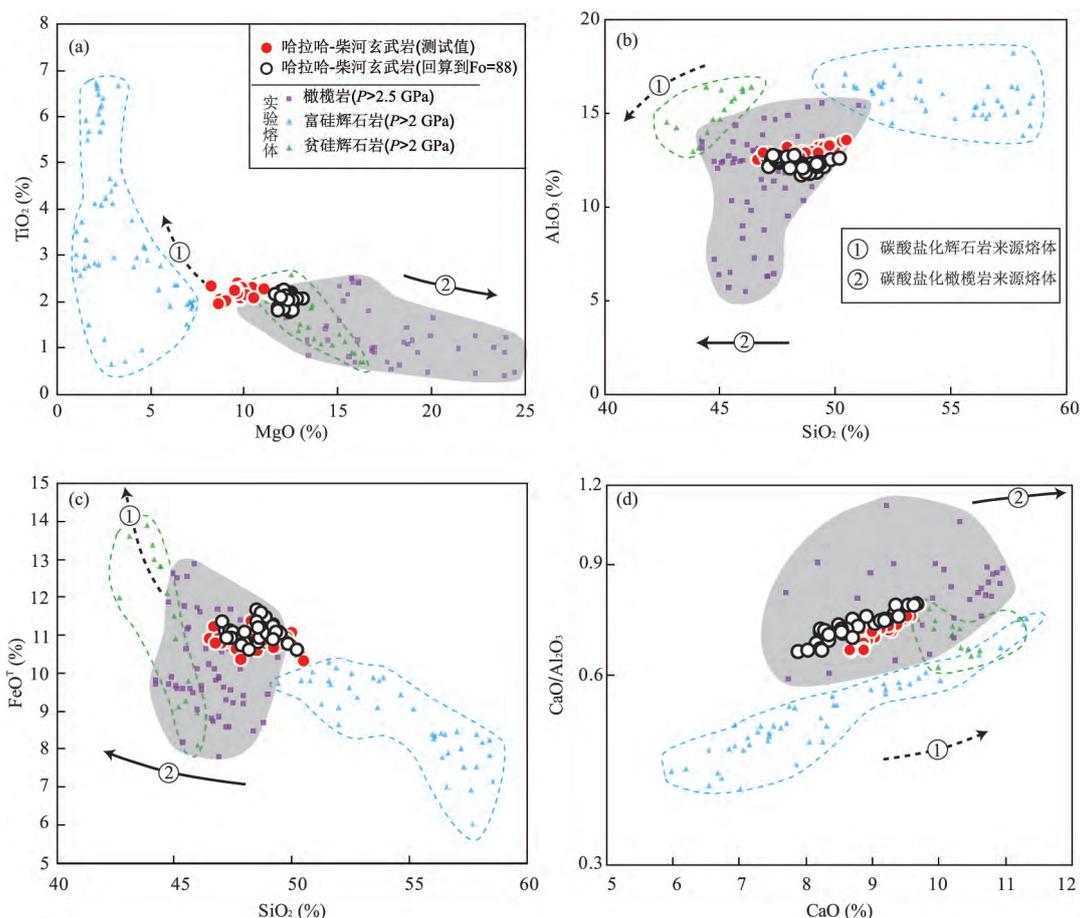


图 8 哈拉哈河—柴河玄武岩与实验熔体在主量元素上的对比:(a)  $MgO - TiO_2$  协变图;(b)  $SiO_2 - Al_2O_3$  协变图;(c)  $SiO_2 - FeO^T$  协变图;(d)  $CaO - (CaO/Al_2O_3)$  协变图

Fig.8 Variation diagrams of (a)  $MgO$  versus  $TiO_2$ ; (b)  $SiO_2$  versus  $Al_2O_3$ ; (c)  $SiO_2$  versus  $FeO^T$ ; (d)  $CaO$  versus  $(CaO/Al_2O_3)$  between the Halaha-Chaihe primary magmas and experimental melt

$>2.5$  GPa 的实验橄榄岩熔体数据引自 Davis *et al.* (2011)、Hirose and Kushiro (1993)、Kushiro (2013)和 Walter (1998);  $>2$  GPa 的贫硅辉石岩熔体数据引自 Hirschmann *et al.* (2003)、Keshav *et al.* (2004)和 Kogiso *et al.* (2003);  $>2$  GPa 的富硅辉石岩熔体数据引自 Pertermann and Hirschmann (2003)、Spandler *et al.* (2007)、Yasuda *et al.* (1994)、Yaxley and Green (1998)和 Yaxley and Sobolev (2007)

体的  $\text{SiO}_2$  含量会显著降低、 $\text{CaO}$  含量会显著升高,而哈拉哈河—柴河玄武岩的原始岩浆的组成没有这样的演化趋势(图 8),再次表明岩浆源区未受到碳酸盐物质的明显影响。

位于研究区中部驼峰岭火山锥样品的  $\Sigma\text{REE}$  明显高于大多数样品,且轻、重稀土元素分馏程度更大,样品的  $\delta^{26}\text{Mg}$  值 ( $-0.34 \pm 0.02\%$ , Li *et al.* (2017)) 低于正常地幔的  $\delta^{26}\text{Mg}$  值 ( $\delta^{26}\text{Mg} = -0.25\% \pm 0.04\%$ , Teng (2017)), 暗示驼峰岭样品可能来源于碳酸盐化的地幔源区。而来自德勒河流域样品的  $\Sigma\text{REE}$  则低于平均值,轻、重稀土元素分馏程度较弱,样品的  $\delta^{26}\text{Mg}$  值 ( $-0.19 \pm 0.02\%$ , Li *et al.* (2017)) 则略高于正常地幔值(图 4)。Chen *et al.* (2017) 对德勒河样品的研究发现,此处样品的氧同位素组成明显低于哈拉哈河—柴河地区其他样品,此外在稀土元素球粒陨石标准化图(图 4)上可以观察到明显的 Eu 正异常,暗示岩浆源区可能具有以低  $\delta^{18}\text{O}$  值为特征的再循环下洋壳辉长质组分。驼峰岭和德勒河都位于哈拉哈河—柴河火山区的中心区域。而本次研究的样品都位于哈拉哈河—柴河火山区的外围,在稀土元素球粒陨石标准化图上明显区别于驼峰岭和德勒河的样品(图 4)。因此,该火山区的地幔源区在空间上是不均一的,可能仅在中心区含有再循环的地壳物质。

#### 4.3 微量元素模拟计算

为了验证大兴安岭地区哈拉哈河—柴河新生代玄武岩的微量元素特征(如富集大离子亲石元素和 Nb、Ta 的正异常)是否可由橄榄岩经部分熔融形成,我们假定源岩具有原始地幔或亏损地幔的化学组成,并分别进行了批式部分熔融作用的微量元素模拟计算(图 9,附表 4)。

樊祺诚等(2008)对哈拉哈河—柴河地区玄武岩中发现的地幔捕虏体进行  $P$ - $T$  平衡条件估算,发现其形成于尖晶石二辉橄榄岩与石榴石二辉橄榄岩相转变带之下,且深度超过 70 km。作为这些地幔捕虏体的寄主岩,其岩浆源区深度至少要大于 70 km,位于石榴子石相的稳定区。因此本文选择石榴子石二辉橄榄岩作为微量元素部分熔融模拟计算的原岩。本文分别选取原始地幔和亏损地幔的微量元素组成作为源岩的初始微量元素组成进行模拟计算。当以原始地幔的微量元素组成(McDonough and Sun, 1995)作为源岩初始微量元素组成时,假定橄榄石、单斜辉石、斜方辉石和石榴子石的矿物比例为 0.40 : 0.20 : 0.33 : 0.07。源岩发生的低程度批式部

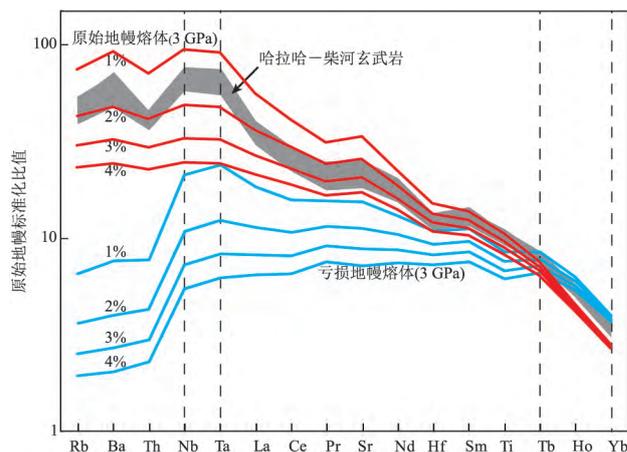


图 9 地幔不同成分批式熔融微量元素模拟计算结果

Fig.9 Results of trace element batch partial melting modeling of different mantle compositions

计算参数见附表 4

分熔融(1%~2%)可以产生具有类似哈拉哈河—柴河玄武岩微量元素特征的熔体。当以亏损地幔的微量元素组成(Workman and Hart, 2005)作为源岩初始微量元素组成时,假定橄榄石、单斜辉石、斜方辉石和石榴子石的矿物比例为 0.62 : 0.15 : 0.20 : 0.03。源岩部分熔融产生的熔体微量元素特征明显区别于哈拉哈河—柴河玄武岩,尤其是强不相容元素含量明显低于哈拉哈河—柴河玄武岩。我们选择饱满的原始地幔组分进行批式部分熔融计算,模拟结果能够获得与研究区玄武岩一致的微量元素组成,反映这种饱满的原始地幔组分发生部分熔融可以形成类似哈拉哈河—柴河玄武岩的熔体。

上述微量元素模拟计算表明源区应该是成分饱满的石榴子石二辉橄榄岩,而岩石圈地幔主要由亏损的橄榄岩组成,显然,哈拉哈河—柴河玄武岩的源区更可能来自于软流圈地幔(而不是岩石圈地幔)。

#### 4.4 哈拉哈河—柴河玄武岩源岩的属性

洋岛玄武岩的成因与起源于核—幔边界的地幔柱活动密切相关,其中具有高 $^3\text{He}/^4\text{He}$ 比值特征的洋岛玄武岩往往被认为是研究下地幔物质组成的理想样品,因为在地球的演化过程中只有下地幔才可能没有经历充分去气的过程,从而有机会保存原始地幔物质(Jackson *et al.*, 2010)。本研究收集整理了全球具有高 $^3\text{He}/^4\text{He}$ 比值( $> 30 R_a$ ,  $R_a$  代表现在大气中的 $^3\text{He}/^4\text{He}$ 比值,约  $1.38 \times 10^{-6}$ )特征的洋岛玄武岩的 Sr、Nd、Pb、Hf 同位素数据(图 6)。来自巴芬岛(Jackson *et al.*, 2010)、西格陵兰(Graham *et al.*, 1998)、夏威夷(Kurz *et al.*, 1982)、加拉帕戈斯(Saal *et*

al., 2007)、萨摩亚(Jackson *et al.*, 2007)、冰岛(Hilton *et al.*, 1999; Stuart *et al.*, 2003; Starkey *et al.*, 2009)和留尼汪群岛(Graham *et al.*, 1990)等地的洋岛玄武岩具有亏损的 Sr-Nd 同位素组成 ( $^{87}\text{Sr}/^{86}\text{Sr} = 0.7030 \sim 0.7046$ ,  $\epsilon_{\text{Nd}} = 3.80 \sim 10.16$ ) 和中等的放射成因 Pb 同位素组成 ( $^{206}\text{Pb}/^{204}\text{Pb} = 17.74 \sim 19.19$ ,  $^{207}\text{Pb}/^{204}\text{Pb} = 15.38 \sim 15.59$ ,  $^{208}\text{Pb}/^{204}\text{Pb} = 37.51 \sim 39.20$ ) (图 1, 图 6). 与中国东部新生代玄武岩对比, 发现大多数东北和华北样品则没有这样的同位素组成, 而只有哈拉哈河—柴河玄武岩 (以及部分华南样品) 的 Sr-Nd-Pb 同位素特征 ( $^{87}\text{Sr}/^{86}\text{Sr} = 0.7035 \sim 0.7039$ ,  $\epsilon_{\text{Nd}} = 5.21 \sim 6.55$ ,  $^{206}\text{Pb}/^{204}\text{Pb} = 18.37 \sim 18.57$ ,  $^{207}\text{Pb}/^{204}\text{Pb} = 15.52 \sim 15.54$ ,  $^{208}\text{Pb}/^{204}\text{Pb} = 38.24 \sim 38.43$ ) 与这些玄武岩极为相似 (图 1). 这些具有高  $^3\text{He}/^4\text{He}$  比特征 ( $^3\text{He}/^4\text{He} > 30R_a$ ) 的洋岛玄武岩被认为受到了深部原始地幔 (而不是亏损地幔) 来源物质的贡献, 反映源区含有深部地幔的物质 (Kurz *et al.*, 1982; Jackson *et al.*, 2010). 因此, 同位素特征的相似性暗示了哈拉哈河—柴河玄武岩源区也存在古老原始地幔物质的参与.

这些具有高  $^3\text{He}/^4\text{He}$  比值特征的洋岛玄武岩具有比球粒陨石样品亏损得多的 Nd 同位素组成, 这可能是由于地球原始 Nd 同位素组成本来就比较亏损, 也可能是因为在地球演化早期 ( $> 4.53$  Ga) 发生了 Nd 同位素的分馏 (Boyet and Carlsw, 2005), 形成了早期 Nd 亏损的地幔储库 (Early Depleted Reservoir, EDR;  $\epsilon_{\text{Nd}} = 5 \sim 9$ ). 哈拉哈河—柴河玄武岩样品的 Nd 同位素组成与 EDR 一致 (图 1a), 暗示古老的地幔物质加入到东北软流圈地幔之中. 研究区玄武岩样品  $^{206}\text{Pb}/^{204}\text{Pb}$  与  $^{207}\text{Pb}/^{204}\text{Pb}$  比值均一, 在  $^{206}\text{Pb}/^{204}\text{Pb} - ^{207}\text{Pb}/^{204}\text{Pb}$  相关图上落在北半球参考线 (Vervoort *et al.*, 2011) 线上或上方, 均落入  $T = 4.42$  Ga ( $(^{206}\text{Pb}/^{204}\text{Pb}) = 0.565 \times (^{207}\text{Pb}/^{204}\text{Pb}) + 5.04$ ) 和  $T = 4.45$  Ga ( $(^{206}\text{Pb}/^{204}\text{Pb}) = 0.577 \times (^{207}\text{Pb}/^{204}\text{Pb}) + 4.92$ ) 的地球等时线之间 (图 6c), 远远早于全球大洋玄武岩的等时年龄  $2.0 \pm 0.3$  Ga (Sun, 1980). 这指示了哈拉哈河—柴河玄武岩源区长期孤立于地球地幔对流造成的铅同位素混合作用 (Allègre and Lewin, 1995), 分离事件很可能发生在地球形成早期 (Jackson *et al.*, 2010).

## 5 结论

(1) 大兴安岭地区哈拉哈河—柴河流域主要出

露新生代火山岩. 主要类型为钠质系列碱性粗面玄武岩和玄武岩, 它们富集大离子亲石元素 (LILEs), 具有明显的 Nb、Ta 正异常, 具有中等亏损的 Sr-Nd-Hf 同位素组成, 且其放射性成因同位素组成均落入高  $^3\text{He}/^4\text{He}$  比值洋岛玄武岩 ( $^3\text{He}/^4\text{He} > 30R_a$ ) 的范围内, 暗示其源区存在古老原始地幔物质的参与;

(2) 与高压实验熔体数据的对比发现, 哈拉哈河—柴河玄武岩的原始岩浆与石榴子石二辉橄榄岩来源熔体在主量元素组成上类似, 暗示玄武岩的源区岩性可能为橄榄岩;

(3) 微量元素模拟计算表明, 在高压环境下以原始地幔为初始成分 (而不是亏损地幔), 经低程度部分熔融 (1%~2%) 产生的熔体具有与哈拉哈河—柴河玄武岩一致的微量元素配分曲线, 支持其源区岩性为饱满的石榴子石二辉橄榄岩.

致谢: 感谢两位匿名审稿专家提出了建设性的审稿意见!

附表 1~4 见本刊官网 (<http://www.earth-science.net>).

## References

- Adam, J., Green, T., 2006. Trace Element Partitioning between Mica- and Amphibole-Bearing Garnet Lherzolite and Hydrous Basaltic Melt: 1. Experimental Results and the Investigation of Controls on Partitioning Behaviour. *Contributions to Mineralogy and Petrology*, 152 (1): 1 - 17. <https://doi.org/10.1007/s00410-006-0085-4>
- Allègre, C. J., Lewin, E., 1995. Isotopic Systems and Stirring Times of the Earth's Mantle. *Earth and Planetary Science Letters*, 136 (3-4): 629 - 646. [https://doi.org/10.1016/0012-821x\(95\)00184-e](https://doi.org/10.1016/0012-821x(95)00184-e)
- Anders, E., Grevesse, N., 1989. Abundances of the Elements: Meteoritic and Solar. *Geochimica et Cosmochimica Acta*, 53 (1): 197 - 214. [https://doi.org/10.1016/0016-7037\(89\)90286-x](https://doi.org/10.1016/0016-7037(89)90286-x)
- Bouvier, A., Vervoort, J. D., Patchett, P. J., 2008. The Lu-Hf and Sm-Nd Isotopic Composition of CHUR: Constraints from Unequilibrated Chondrites and Implications for the Bulk Composition of Terrestrial Planets. *Earth and Planetary Science Letters*, 273 (1-2): 48 - 57. <https://doi.org/10.1016/j.epsl.2008.06.010>
- Boyet, M., Carlsw, R. W., 2005.  $^{142}\text{Nd}$  Evidence for Early ( $> 4.53$  Ga) Global Differentiation of the Silicate Earth. *Science*, 309 (5734): 576 - 581. <https://doi.org/10.1126/science.1113634>

- Chen, H., Xia, Q. K., Ingrin, J., et al., 2017. Heterogeneous Source Components of Intraplate Basalts from NE China Induced by the Ongoing Pacific Slab Subduction. *Earth and Planetary Science Letters*, 459: 208–220. <https://doi.org/10.1016/j.epsl.2016.11.030>
- Chen, L. H., Zeng, G., Hu, S. L., et al., 2012. Crustal Recycling and Genesis of Continental Alkaline Basalts: Case Study of the Cenozoic Alkaline Basalts from Shandong Province, Eastern China. *Geological Journal of China Universities*, 18(1): 16–27 (in Chinese with English abstract).
- Chen, L. H., Zeng, G., Jiang, S. Y., et al., 2009. Sources of Anfengshan Basalts: Subducted Lower Crust in the Sulu UHP Belt, China. *Earth and Planetary Science Letters*, 286(3–4): 426–435. <https://doi.org/10.1016/j.epsl.2009.07.006>
- Chen, X. Y., Chen, L. H., Chen, Y., et al., 2014. Distribution Summary of Cenozoic Basalts in Central and Eastern China. *Geological Journal of China Universities*, 20(4): 507–519 (in Chinese with English abstract).
- Chu, Z. Y., Harvey, J., Liu, C. Z., et al., 2013. Source of Highly Potassic Basalts in Northeast China: Evidence from Re-Os, Sr-Nd-Hf Isotopes and PGE Geochemistry. *Chemical Geology*, 357: 52–66. <https://doi.org/10.1016/j.chemgeo.2013.08.007>
- Davis, F. A., Hirschmann, M. M., Humayun, M., 2011. The Composition of the Incipient Partial Melt of Garnet Peridotite at 3 GPa and the Origin of OIB. *Earth and Planetary Science Letters*, 308(3–4): 380–390. <https://doi.org/10.1016/j.epsl.2011.06.008>
- Fan, Q., Hooper, P. R., 1991. The Cenozoic Basaltic Rocks of Eastern China: Petrology and Chemical Composition. *Journal of Petrology*, 32(4): 765–810. <https://doi.org/10.1093/petrology/32.4.765>
- Fan, Q. C., Sui, J. L., Zhao, Y. W., et al., 2008. Preliminary Study on Garnet Peridotite Xenolith of Quaternary Volcanic Rocks in Middle Daxing'an Mountain Range. *Acta Petrologica Sinica*, 24(11): 2563–2568 (in Chinese with English abstract).
- Fan, Q. C., Zhao, Y. W., Li, D. M., et al., 2011. Studies on Quaternary Volcanism Stages of Halaha River and Chaoer River Area in the Great Xing'an Range: Evidence from K-Ar Dating and Volcanic Geology Features. *Acta Petrologica Sinica*, 27(10): 2827–2832 (in Chinese with English abstract).
- Gale, A., Dalton, C. A., Langmuir, C. H., et al., 2013. The Mean Composition of Ocean Ridge Basalts. *Geochemistry, Geophysics, Geosystems*, 14(3): 489–518. <https://doi.org/10.1029/2012gc004334>
- Geske, A., Goldstein, R. H., Mavromatis, V., et al., 2015. The Magnesium Isotope ( $\delta^{26}\text{Mg}$ ) Signature of Dolomites. *Geochimica et Cosmochimica Acta*, 149: 131–151. <https://doi.org/10.1016/j.gca.2014.11.003>
- Graham, D. W., Larsen, L. M., Hanan, B. B., et al., 1998. Helium Isotope Composition of the Early Iceland Mantle Plume Inferred from the Tertiary Picrites of West Greenland. *Earth and Planetary Science Letters*, 160(3–4): 241–255. [https://doi.org/10.1016/s0012-821x\(98\)00083-1](https://doi.org/10.1016/s0012-821x(98)00083-1)
- Graham, D., Lupton, J., Albarède, F., et al., 1990. Extreme Temporal Homogeneity of Helium Isotopes at Piton de la Fournaise, Réunion Island. *Nature*, 347(6293): 545–548. <https://doi.org/10.1038/347545a0>
- Green, T. H., Blundy, J. D., Adam, J., et al., 2000. SIMS Determination of Trace Element Partition Coefficients between Garnet, Clinopyroxene and Hydrous Basaltic Liquids at 2–7.5 GPa and 1 080–1 200 °C. *Lithos*, 53(3–4): 165–187. [https://doi.org/10.1016/s0024-4937\(00\)00023-2](https://doi.org/10.1016/s0024-4937(00)00023-2)
- Hart, S. R., 1984. A Large-Scale Isotope Anomaly in the Southern Hemisphere Mantle. *Nature*, 309(5971): 753–757. <https://doi.org/10.1038/309753a0>
- Hilton, D. R., Grönvold, K., MacPherson, C. G., et al., 1999. Extreme  $^3\text{He}/^4\text{He}$  Ratios in Northwest Iceland: Constraining the Common Component in Mantle Plumes. *Earth and Planetary Science Letters*, 173(1/2): 53–60. [https://doi.org/10.1016/s0012-821x\(99\)00215-0](https://doi.org/10.1016/s0012-821x(99)00215-0)
- Hirose, K., Kushiro, I., 1993. Partial Melting of Dry Peridotites at High Pressures: Determination of Compositions of Melts Segregated from Peridotite Using Aggregates of Diamond. *Earth and Planetary Science Letters*, 114(4): 477–489. [https://doi.org/10.1016/0012-821x\(93\)90077-m](https://doi.org/10.1016/0012-821x(93)90077-m)
- Hirschmann, M. M., Kogiso, T., Baker, M. B., et al., 2003. Alkaline Magmas Generated by Partial Melting of Garnet Pyroxenite. *Geology*, 31(6): 481. [https://doi.org/10.1130/0091-7613\(2003\)0310481:amgbpm>2.0.co;2](https://doi.org/10.1130/0091-7613(2003)0310481:amgbpm>2.0.co;2)
- Ho, K. S., Ge, W. C., Chen, J. C., et al., 2013. Late Cenozoic Magmatic Transitions in the Central Great Xing'an Range, Northeast China: Geochemical and Isotopic Constraints on Petrogenesis. *Chemical Geology*, 352: 1–18. <https://doi.org/10.1016/j.chemgeo.2013.05.040>
- Ho, K. S., Liu, Y., Chen, J. C., et al., 2008. Elemental and Sr-Nd-Pb Isotopic Compositions of Late Cenozoic Abaga Basalts, Inner Mongolia: Implications for Petrogenesis and Mantle Process. *Geochemical Journal*, 42(4): 339–357. <https://doi.org/10.2343/geochemj.42.339>
- Hofmann, A. W., 1997. Mantle Geochemistry: The Message from Oceanic Volcanism. *Nature*, 385(6613): 219–229. <https://doi.org/10.1038/385219a0>
- Hofmann, A. W., Jochum, K. P., Seufert, M., et al., 1986. Nb and

- Pb in Oceanic Basalts: New Constraints on Mantle Evolution. *Earth and Planetary Science Letters*, 79(1–2): 33–45. [https://doi.org/10.1016/0012-821x\(86\)90038-5](https://doi.org/10.1016/0012-821x(86)90038-5)
- Holmes, A., 1946. An Estimate of the Age of the Earth. *Nature*, 157(3995): 680–684. <https://doi.org/10.1038/157680a0>
- Hong, L. B., Zhang, Y. H., Qian, S. P., et al., 2013. Constraints from Melt Inclusions and Their Host Olivines on the Petrogenesis of Oligocene–Early Miocene Xindian Basalts, Chifeng Area, North China Craton. *Contributions to Mineralogy and Petrology*, 165(2): 305–326. <https://doi.org/10.1007/s00410-012-0810-0>
- Huang, J. L., Zhao, D. P., 2006. High-Resolution Mantle Tomography of China and Surrounding Regions. *Journal of Geophysical Research*, 111(B9): B09305. <https://doi.org/10.1029/2005jb004066>
- Huang, J., Li, S. G., Xiao, Y. L., et al., 2015. Origin of Low  $\delta^{26}\text{Mg}$  Cenozoic Basalts from South China Block and Their Geodynamic Implications. *Geochimica et Cosmochimica Acta*, 164: 298–317. <https://doi.org/10.1016/j.gca.2015.04.054>
- Jackson, M. G., Carlson, R. W., Kurz, M. D., et al., 2010. Evidence for the Survival of the Oldest Terrestrial Mantle Reservoir. *Nature*, 466(7308): 853–856. <https://doi.org/10.1038/nature09287>
- Jackson, M., Kurz, M., Hart, S., et al., 2007. New Samoan Lavas from Ofu Island Reveal a Hemispherically Heterogeneous High  $^3\text{He}/^4\text{He}$  Mantle. *Earth and Planetary Science Letters*, 264(3–4): 360–374. <https://doi.org/10.1016/j.epsl.2007.09.023>
- Jahn, B. M., Wu, F. Y., Chen, B., 2000. Granitoids of the Central Asian Orogenic Belt and Continental Growth in the Phanerozoic. *Geological Society of America, Special Paper*, 350: 181–193. <https://doi.org/10.1130/0-8137-2350-7.181>
- Jochum, K. P., Weis, U., Schwager, B., et al., 2016. Reference Values Following ISO Guidelines for Frequently Requested Rock Reference Materials. *Geostandards and Geoanalytical Research*, 40(3): 333–350. <https://doi.org/10.1111/j.1751-908x.2015.00392.x>
- Keshav, S., Gudfinnsson, G. H., Sen, G., et al., 2004. High-Pressure Melting Experiments on Garnet Clinopyroxenite and the Alkalic to Tholeiitic Transition in Ocean-Island Basalts. *Earth and Planetary Science Letters*, 223(3–4): 365–379. <https://doi.org/10.1016/j.epsl.2004.04.029>
- Kogiso, T., Hirschmann, M. M., Frost, D. J., 2003. High-Pressure Partial Melting of Garnet Pyroxenite: Possible Mafic Lithologies in the Source of Ocean Island Basalts. *Earth and Planetary Science Letters*, 216(4): 603–617. [https://doi.org/10.1016/s0012-821x\(03\)00538-7](https://doi.org/10.1016/s0012-821x(03)00538-7)
- Kuritani, T., Kimura, J. I., Miyamoto, T., et al., 2009. Intraplate Magmatism Related to Deceleration of Upwelling Asthenospheric Mantle: Implications from the Changbaishan Shield Basalts, Northeast China. *Lithos*, 112(3–4): 247–258. <https://doi.org/10.1016/j.lithos.2009.02.007>
- Kuritani, T., Kimura, J. I., Ohtani, E., et al., 2013. Transition Zone Origin of Potassic Basalts from Wudalianchi Volcano, Northeast China. *Lithos*, 156–159: 1–12. <https://doi.org/10.1016/j.lithos.2012.10.010>
- Kuritani, T., Nakamura, E., 2002. Precise Isotope Analysis of Nanogram-Level Pb for Natural Rock Samples without Use of Double Spikes. *Chemical Geology*, 186(1–2): 31–43. [https://doi.org/10.1016/s0009-2541\(02\)00004-9](https://doi.org/10.1016/s0009-2541(02)00004-9)
- Kuritani, T., Ohtani, E., Kimura, J. I., 2011. Intensive Hydration of the Mantle Transition Zone beneath China Caused by Ancient Slab Stagnation. *Nature Geoscience*, 4(10): 713–716. <https://doi.org/10.1038/ngeo1250>
- Kurz, M. D., Jenkins, W. J., Hart, S. R., 1982. Helium Isotopic Systematics of Oceanic Islands and Mantle Heterogeneity. *Nature*, 297(5861): 43–47. <https://doi.org/10.1038/297043a0>
- Kushiro, I., 2013. Partial Melting of a Fertile Mantle Peridotite at High Pressures: An Experimental Study Using Aggregates of Diamond. In: Kushiro, I., ed., *Earth Processes: Reading the Isotopic Code*. American Geophysical Union, Washington, D. C., 109–122. <https://doi.org/10.1029/gm095p0109>
- Le Bas, M. J., Le Maitre, R. W., Streckeisen, A., et al., 1986. A Chemical Classification of Volcanic Rocks Based on the Total Alkali-Silica Diagram. *Journal of Petrology*, 27(3): 745–750. <https://doi.org/10.1093/petrology/27.3.745>
- Li, H. Y., Xu, Y. G., Ryan, J. G., et al., 2017. Olivine and Melt Inclusion Chemical Constraints on the Source of Intracontinental Basalts from the Eastern North China Craton: Discrimination of Contributions from the Subducted Pacific Slab. *Geochimica et Cosmochimica Acta*, 178: 1–19. <https://doi.org/10.1016/j.gca.2015.12.032>
- Li, S. G., Yang, W., Ke, S., et al., 2016. Deep Carbon Cycles Constrained by a Large-Scale Mantle Mg Isotope Anomaly in Eastern China. *National Science Review*, 4(1): 111–120. <https://doi.org/10.1093/nsr/nww070>
- Li, Y. Q., Ma, C. Q., Robinson, P. T., et al., 2015. Recycling of Oceanic Crust from a Stagnant Slab in the Mantle Transition Zone: Evidence from Cenozoic Continental Basalts in Zhejiang Province, SE China. *Lithos*, 230: 146–165. <https://doi.org/10.1016/j.lithos.2015.05.021>
- Liu, J. Q., Chen, L. H., Wang, X. J., et al., 2017. The Role of Melt-Rock Interaction in the Formation of Quaternary

- High-MgO Potassic Basalt from the Greater Khingan Range, Northeast China. *Journal of Geophysical Research; Solid Earth*, 122 (1): 262 – 280. <https://doi.org/10.1002/2016jb013605>
- Liu, J. Q., Ren, Z. Y., Nichols, A. R. L., et al., 2015. Petrogenesis of Late Cenozoic Basalts from North Hainan Island: Constraints from Melt Inclusions and Their Host Olivines. *Geochimica et Cosmochimica Acta*, 152: 89 – 121. <https://doi.org/10.1016/j.gca.2014.12.023>
- Liu, S. A., Wang, Z. Z., Li, S. G., et al., 2016. Zinc Isotope Evidence for a Large-Scale Carbonated Mantle beneath Eastern China. *Earth and Planetary Science Letters*, 444: 169 – 178. <https://doi.org/10.1016/j.epsl.2016.03.051>
- Liu, R. X., 1992. Geochronology and Geochemistry of Cenozoic Volcanic Rocks in China. Seismological Press, Beijing (in Chinese).
- McDonough, W. F., Sun, S. S., 1995. The Composition of the Earth. *Chemical Geology*, 120 (3 – 4): 223 – 253. [https://doi.org/10.1016/0009-2541\(94\)00140-4](https://doi.org/10.1016/0009-2541(94)00140-4)
- Meng, F. C., Safonova, I., Chen, S. S., et al., 2018. Late Cenozoic Intra-Plate Basalts of the Greater Khingan Range in NE China and Khangai Province in Central Mongolia. *Gondwana Research*, 63: 65 – 84. <https://doi.org/10.1016/j.gr.2018.05.009>
- Pertermann, M., Hirschmann, M. M., 2003. Anhydrous Partial Melting Experiments on MORB-Like Eclogite: Phase Relations, Phase Compositions and Mineral-Melt Partitioning of Major Elements at 2–3 GPa. *Journal of Petrology*, 44(12): 2173 – 2201. <https://doi.org/10.1093/ptrology/egg074>
- Pu, W., Gao, J. F., Zhao, K. D., et al., 2005. Separation Method of Rb-Sr, Sm-Nd Using DCTA and HIBA. *Journal of Nanjing University (Natural Sciences)*, 41(4): 445 – 450 (in Chinese with English abstract).
- Roeder, P. L., Emslie, R. F., 1970. Olivine-Liquid Equilibrium. *Contributions to Mineralogy and Petrology*, 29 (4): 275 – 289. <https://doi.org/10.1007/bf00371276>
- Rudnick, R. L., Gao, S., 2003. Composition of the Continental Crust. In: Rudnick, R. L., Gao, S., eds., *Treatise on Geochemistry*. Elsevier, Cambridge, 1 – 64. <https://doi.org/10.1016/b0-08-043751-6/03016-4>
- Saal, A., Kurz, M., Hart, S., et al., 2007. The Role of Lithospheric Gabbros on the Composition of Galapagos Lavas. *Earth and Planetary Science Letters*, 257(3 – 4): 391 – 406. <https://doi.org/10.1016/j.epsl.2007.02.040>
- Saenger, C., Wang, Z. R., 2014. Magnesium Isotope Fractionation in Biogenic and Abiogenic Carbonates: Implications for Paleoenvironmental Proxies. *Quaternary Science Reviews*, 90: 1 – 21. <https://doi.org/10.1016/j.quascirev.2014.01.014>
- Spandler, C., Yaxley, G., Green, D. H., et al., 2007. Phase Relations and Melting of Anhydrous K-Bearing Eclogite from 1 200 to 1 600 °C and 3 to 5 GPa. *Journal of Petrology*, 49(4): 771 – 795.
- Starkey, N. A., Stuart, F. M., Ellam, R. M., et al., 2009. Helium Isotopes in Early Iceland Plume Picrites: Constraints on the Composition of High <sup>3</sup>He/<sup>4</sup>He Mantle. *Earth and Planetary Science Letters*, 277(1 – 2): 91 – 100. <https://doi.org/10.1016/j.epsl.2008.10.007>
- Stracke, A., 2012. Earth's Heterogeneous Mantle: A Product of Convection-Driven Interaction between Crust and Mantle. *Chemical Geology*, 330/331: 274 – 299. <https://doi.org/10.1016/j.chemgeo.2012.08.007>
- Stuart, F. M., Lass-Evans, S., Godfrey Fitton, J., et al., 2003. High <sup>3</sup>He/<sup>4</sup>He Ratios in Picritic Basalts from Baffin Island and the Role of a Mixed Reservoir in Mantle Plumes. *Nature*, 424 (6944): 57 – 59. <https://doi.org/10.1038/nature01711>
- Sun, S. S., 1980. Lead Isotopic Study of Young Volcanic Rocks from Mid-Ocean Ridges, Ocean Islands and Island Arcs. *Philosophical Transactions of the Royal Society A: Mathematical, Physical and Engineering Sciences*, 297(1431): 409 – 445. <https://doi.org/10.1098/rsta.1980.0224>
- Sun, Y. B., Zhang, R., Ding, C. C., et al., 2016. Adsorption of U (VI) on Sericite in the Presence of Bacillus Subtilis: A Combined Batch, EXAFS and Modeling Techniques. *Geochimica et Cosmochimica Acta*, 180: 51 – 65. <https://doi.org/10.1016/j.gca.2016.02.012>
- Sun, Y., Ying, J. F., Su, B. X., et al., 2015. Contribution of Crustal Materials to the Mantle Sources of Xiaogulihe Ultrapotassic Volcanic Rocks, Northeast China: New Constraints from Mineral Chemistry and Oxygen Isotopes of Olivine. *Chemical Geology*, 405: 10 – 18. <https://doi.org/10.1016/j.chemgeo.2015.04.005>
- Tang, Y. J., Zhang, H. F., Nakamura, E., et al., 2007. Lithium Isotopic Systematics of Peridotite Xenoliths from Hannuoba, North China Craton: Implications for Melt-Rock Interaction in the Considerably Thinned Lithospheric Mantle. *Geochimica et Cosmochimica Acta*, 71(17): 4327 – 4341. <https://doi.org/10.1016/j.gca.2007.07.006>
- Tao, K., Niu, F. L., Ning, J. Y., et al., 2014. Crustal Structure beneath NE China Imaged by NECESSArray Receiver Function Data. *Earth and Planetary Science Letters*, 398: 48 – 57. <https://doi.org/10.1016/j.epsl.2014.04.043>
- Teng, F. Z., 2017. Magnesium Isotope Geochemistry. *Reviews in Mineralogy and Geochemistry*, 82 (1): 219 – 287. <https://doi.org/10.2138/rmg.2017.82.7>

- Teng, F.Z., Li, W.Y., Ke, S., et al., 2010. Magnesium Isotopic Composition of the Earth and Chondrites. *Geochimica et Cosmochimica Acta*, 74 (14): 4150 – 4166. <https://doi.org/10.1016/j.gca.2010.04.019>
- Vervoort, J.D., Plank, T., Prytulak, J., 2011. The Hf-Nd Isotopic Composition of Marine Sediments. *Geochimica et Cosmochimica Acta*, 75 (20): 5903 – 5926. <https://doi.org/10.1016/j.gca.2011.07.046>
- Walter, M.J., 1998. Melting of Garnet Peridotite and the Origin of Komatiite and Depleted Lithosphere. *Journal of Petrology*, 39(1): 29 – 60. <https://doi.org/10.1093/pe-trology/39.1.29>
- Wang, X.J., Chen, L.H., Hofmann, A.W., et al., 2017. Mantle Transition Zone-Derived EM1 Component beneath NE China: Geochemical Evidence from Cenozoic Potassic Basalts. *Earth and Planetary Science Letters*, 465: 16 – 28. <https://doi.org/10.1016/j.epsl.2017.02.028>
- Wang, Y., Zhao, Z.F., Zheng, Y.F., et al., 2011. Geochemical Constraints on the Nature of Mantle Source for Cenozoic Continental Basalts in East-Central China. *Lithos*, 125 (3 – 4): 940 – 955. <https://doi.org/10.1016/j.lithos.2011.05.007>
- Wei, W., Xu, J.D., Zhao, D.P., et al., 2012. East Asia Mantle Tomography: New Insight into Plate Subduction and Intraplate Volcanism. *Journal of Asian Earth Sciences*, 60: 88 – 103. <https://doi.org/10.1016/j.jseas.2012.08.001>
- Weis, D., Kieffer, B., Maerschalk, C., et al., 2006. High-Precision Isotopic Characterization of USGS Reference Materials by TIMS and MC-ICP-MS. *Geochemistry, Geophysics, Geosystems*, 7 (8). <https://doi.org/10.1029/2006gc001283>
- Wombacher, F., Eisenhauer, A., Böhm, F., et al., 2011. Magnesium Stable Isotope Fractionation in Marine Biogenic Calcite and Aragonite. *Geochimica et Cosmochimica Acta*, 75 (19): 5797 – 5818. <https://doi.org/10.1016/j.gca.2011.07.017>
- Workman, R.K., Hart, S.R., 2005. Major and Trace Element Composition of the Depleted MORB Mantle (DMM). *Earth and Planetary Science Letters*, 231 (1 – 2): 53 – 72. <https://doi.org/10.1016/j.epsl.2004.12.005>
- Xiao, W.J., Windley, B.F., Sun, S., et al., 2015. A Tale of Amalgamation of Three Permo-Triassic Collage Systems in Central Asia: Oroclines, Sutures, and Terminal Accretion. *Annual Review of Earth and Planetary Sciences*, 43 (1): 477 – 507. <https://doi.org/10.1146/annurev-earth-060614-105254>
- Xu, Y.G., 2007. Diachronous Lithospheric Thinning of the North China Craton and Formation of the Daxin'anling-Taihangshan Gravity Lineament. *Lithos*, 96 (1 – 2): 281 – 298. <https://doi.org/10.1016/j.lithos.2006.09.013>
- Xu, Y.G., Li, H.Y., Hong, L.B., et al., 2018. Generation of Cenozoic Intraplate Basalts in the Big Mantle Wedge under Eastern Asia. *Science China Earth Sciences*, 48 (7): 825 – 843 (in Chinese).
- Xu, Y.G., Zhang, H.H., Qiu, H.N., et al., 2012. Oceanic Crust Components in Continental Basalts from Shuangliao, Northeast China: Derived from the Mantle Transition Zone? *Chemical Geology*, 328: 168 – 184. <https://doi.org/10.1016/j.chemgeo.2012.01.027>
- Xu, Z., Zheng, Y.F., Zhao, Z.F., 2017. The Origin of Cenozoic Continental Basalts in East-Central China: Constrained by Linking Pb Isotopes to Other Geochemical Variables. *Lithos*, 268 – 271: 302 – 319. <https://doi.org/10.1016/j.lithos.2016.11.006>
- Yang, W., Teng, F.Z., Zhang, H.F., et al., 2012. Magnesium Isotopic Systematics of Continental Basalts from the North China Craton: Implications for Tracing Subducted Carbonate in the Mantle. *Chemical Geology*, 328: 185 – 194. <https://doi.org/10.1016/j.chemgeo.2012.05.018>
- Yang, Y.H., Zhang, H.F., Chu, Z.Y., et al., 2010. Combined Chemical Separation of Lu, Hf, Rb, Sr, Sm and Nd from a Single Rock Digest and Precise and Accurate Isotope Determinations of Lu-Hf, Rb-Sr and Sm-Nd Isotope Systems Using Multi-Collector ICP-MS and TIMS. *International Journal of Mass Spectrometry*, 290 (2 – 3): 120 – 126. <https://doi.org/10.1016/j.ijms.2009.12.011>
- Yang, Z.F., Li, J., Liang, W.F., et al., 2016. On the Chemical Markers of Pyroxenite Contributions in Continental Basalts in Eastern China: Implications for Source Lithology and the Origin of Basalts. *Earth-Science Reviews*, 157: 18 – 31. <https://doi.org/10.1016/j.earscirev.2016.04.001>
- Yasuda, A., Fujii, T., Kurita, K., 1994. Melting Phase Relations of an Anhydrous Mid-Ocean Ridge Basalt from 3 to 20 GPa: Implications for the Behavior of Subducted Oceanic Crust in the Mantle. *Journal of Geophysical Research: Solid Earth*, 99 (B5): 9401 – 9414. <https://doi.org/10.1029/93jb03205>
- Yaxley, G.M., Sobolev, A.V., 2007. High-Pressure Partial Melting of Gabbro and Its Role in the Hawaiian Magma Source. *Contributions to Mineralogy and Petrology*, 154 (4): 371 – 383. <https://doi.org/10.1007/s00410-007-0198-4>
- Yaxley, G.M., Green, D.H., 1998. Reactions between Eclogite and Peridotite: Mantle Refertilisation by Subduction of Oceanic Crust. *Schweiz. Mineral. Petrogr. Mitt.*, 78 (2): 243 – 255.
- Yu, S.Y., Xu, Y.G., Zhou, S.H., et al., 2018. Late Cenozoic Basaltic Lavas from the Changbaishan-Baoqing Volcanic Belt, NE China: Products of Lithosphere-Asthenosphere

- Interaction Induced by Subduction of the Pacific Plate. *Journal of Asian Earth Sciences*, 164: 260 – 273. <https://doi.org/10.1016/j.jseaes.2018.06.031>
- Zeng, G., Chen, L. H., Hofmann, A. W., et al., 2011. Crust Recycling in the Sources of Two Parallel Volcanic Chains in Shandong, North China. *Earth and Planetary Science Letters*, 302 (3 – 4): 359 – 368. <https://doi.org/10.1016/j.epsl.2010.12.026>
- Zeng, G., Chen, L. H., Xu, X. S., et al., 2010. Carbonated Mantle Sources for Cenozoic Intra-Plate Alkaline Basalts in Shandong, North China. *Chemical Geology*, 273 (1 – 2): 35–45. <https://doi.org/10.1016/j.chemgeo.2010.02.009>
- Zeng, G., Chen, L. H., Yu, X., et al., 2017. Magma-Magma Interaction in the Mantle beneath Eastern China. *Journal of Geophysical Research: Solid Earth*, 122(4): 2763 – 2779. <https://doi.org/10.1002/2017jb014023>
- Zhang, J. J., Zheng, Y. F., Zhao, Z. F., 2009. Geochemical Evidence for Interaction between Oceanic Crust and Lithospheric Mantle in the Origin of Cenozoic Continental Basalts in East-Central China. *Lithos*, 110(1): 305–326. <https://doi.org/10.1016/j.lithos.2009.01.006>
- Zhang, L. Y., Prelević, D., Li, N., et al., 2016. Variation of Olivine Composition in the Volcanic Rocks in the Songliao Basin, NE China: Lithosphere Control on the Origin of the K-Rich Intraplate Mafic Lavas. *Lithos*, 262: 153 – 168. <https://doi.org/10.1016/j.lithos.2016.06.028>
- Zhang, M. L., Guo, Z. F., 2016. Origin of Late Cenozoic Abagadaluoe Basalts, Eastern China: Implications for a Mixed Pyroxenite-Peridotite Source Related with Deep Subduction of the Pacific Slab. *Gondwana Research*, 37: 130–151. <https://doi.org/10.1016/j.gr.2016.05.014>
- Zhang, R. Q., Wu, Q. J., Sun, L., et al., 2014. Crustal and Lithospheric Structure of Northeast China from S-Wave Receiver Functions. *Earth and Planetary Science Letters*, 401: 196 – 205. <https://doi.org/10.1016/j.epsl.2014.06.017>
- Zhang, Y. L., Liu, C. Z., Ge, W. C., et al., 2011. Ancient Sub-Continental Lithospheric Mantle (SCLM) beneath the Eastern Part of the Central Asian Orogenic Belt (CAOB): Implications for Crust-Mantle Decoupling. *Lithos*, 126 (3 – 4): 233–247. <https://doi.org/10.1016/j.lithos.2011.07.022>
- Zhao, Y. W., Fan, Q. C., 2011. Characteristics of Lithospheric Mantle beneath the Great Xing'an Range: Evidence from Spinel Peridotite Xenoliths in the Halaha River and Chaoer River Area. *Acta Petrologica Sinica*, 27 (10): 2833–2841 (in Chinese with English abstract).
- Zhao, Y. W., Fan, Q. C., 2012. Mantle Sources and Magma Genesis of Quaternary Volcanic Rocks in the Halaha River and Chaoer River Area, Great Xing'an Range. *Acta Petrologica Sinica*, 28(4): 1119 – 1129 (in Chinese with English abstract).
- Zhao, Y. W., Fan, Q. C., Bai, Z. D., et al., 2008. Preliminary Study on Quaternary Volcanoes in the Halaha River and Chaoer River Area in Daxing'an Mountain Range. *Acta Petrologica Sinica*, 24 (11): 2569 – 2575 (in Chinese with English abstract).
- Zhou, X., Armstrong, R., 1982. Cenozoic Volcanic Rocks of Eastern China: Secular and Geographic Trends in Chemistry and Strontium Isotopic Composition. *Earth and Planetary Science Letters*, 58 (3): 301 – 329. [https://doi.org/10.1016/0012-821x\(82\)90083-8](https://doi.org/10.1016/0012-821x(82)90083-8)
- Zou, H. B., Zindler, A., Xu, X. S., et al., 2000. Major, Trace Element, and Nd, Sr and Pb Isotope Studies of Cenozoic Basalts in SE China: Mantle Sources, Regional Variations, and Tectonic Significance. *Chemical Geology*, 171(1–2): 33 – 47. [https://doi.org/10.1016/s0009-2541\(00\)00243-6](https://doi.org/10.1016/s0009-2541(00)00243-6)

#### 附中文参考文献

- 陈立辉, 曾罡, 胡森林, 等, 2012. 地壳再循环与大陆碱性玄武岩的成因: 以山东新生代碱性玄武岩为例. *高校地质学报*, 18(1): 16–27.
- 陈霞玉, 陈立辉, 陈暘, 等, 2014. 中国中—东部地区新生代玄武岩的分布规律与面积汇总. *高校地质学报*, 20(4): 507–519.
- 樊祺诚, 隋建立, 赵勇伟, 等, 2008. 大兴安岭中部第四纪火山岩中石榴石橄榄岩捕虏体的初步研究. *岩石学报*, 24 (11): 2563–2568.
- 樊祺诚, 赵勇伟, 李大明, 等, 2011. 大兴安岭哈拉哈河—绰尔河第四纪火山分期: K-Ar 年代学与火山地质特征. *岩石学报*, 27(10): 2827–2832.
- 刘若新, 1992. 中国新生代火山岩年代学与地球化学. 北京: 地震出版社.
- 濮巍, 高剑峰, 赵葵东, 等, 2005. 利用 DCTA 和 HIBA 快速有效分离 Rb-Sr, Sm-Nd 的方法. *南京大学学报(自然科学版)*, 41(4): 445–450.
- 徐义刚, 李洪颜, 洪路兵, 等, 2018. 东亚大地幔楔与中国东部新生代板内玄武岩成因. *中国科学: 地球科学*, 48(7): 825–843.
- 赵勇伟, 樊祺诚, 2011. 大兴安岭岩石圈地幔特征: 哈拉哈河—绰尔河橄榄岩捕虏体的证据. *岩石学报*, 27(10): 2833–2841.
- 赵勇伟, 樊祺诚, 2012. 大兴安岭哈拉哈河—绰尔河第四纪火山岩地幔源区与岩浆成因. *岩石学报*, 28(4): 1119–1129.
- 赵勇伟, 樊祺诚, 白志达, 等, 2008. 大兴安岭哈拉哈河—绰尔河地区第四纪火山活动初步研究. *岩石学报*, 24(11): 2569–2575.

附表 1 哈拉哈河-柴河玄武岩全岩主量元素(%)分析结果  
Appendix table 1 Whole rock major elements (%) for Halaha-Chaihe basalts

样品	采样位置	SiO <sub>2</sub>	TiO <sub>2</sub>	Al <sub>2</sub> O <sub>3</sub>	Fe <sub>2</sub> O <sub>3</sub> <sup>Ta</sup>	MnO	MgO	CaO	Na <sub>2</sub> O	K <sub>2</sub> O	P <sub>2</sub> O <sub>5</sub>	LOI	Total	Mg# <sup>b</sup>
13CH05	47°38'05.12"N, 121°15'24.97"E	46.81	2.16	12.67	12.08	0.17	11.08	9.52	3.19	1.56	0.41	-0.10	99.54	65.79
13CH07	47°38'05.07"N, 121°15'24.77"E	46.87	2.19	12.49	12.36	0.17	11.00	9.67	3.25	1.56	0.44	-0.33	99.68	65.11
13CH08	47°39'02.07"N, 121°16'36.30"E	47.09	2.09	12.45	12.04	0.16	11.58	9.65	2.90	1.36	0.41	0.18	99.90	66.85
13CH09	47°39'02.13"N, 121°16'36.26"E	46.67	2.11	12.48	12.05	0.16	11.53	9.71	2.70	1.31	0.40	0.49	99.62	66.74
13CH10	47°39'02.11"N, 121°16'36.39"E	47.04	2.14	12.56	12.05	0.16	11.45	9.73	2.74	1.35	0.42	0.31	99.95	66.58
13CH11	47°39'45.76"N, 121°16'48.79"E	47.58	2.15	12.68	11.93	0.17	11.20	9.34	3.10	1.59	0.44	-0.35	99.82	66.31
13CH12	47°39'51.12"N, 121°16'29.70"E	47.14	2.15	12.84	11.91	0.17	11.02	9.43	3.15	1.60	0.41	-0.18	99.64	65.99
13CH13	47°39'51.07"N, 121°16'29.63"E	46.92	2.16	12.90	11.90	0.17	11.02	9.60	3.10	1.54	0.42	0.08	99.82	66.01
13CH14	47°33'16.71"N, 121°18'10.39"E	48.14	2.19	12.86	11.72	0.16	10.36	9.34	3.15	1.63	0.42	-0.22	99.74	64.96
13CH15	47°33'16.65"N, 121°18'10.08"E	47.84	2.23	12.86	11.74	0.16	10.58	9.43	3.01	1.64	0.43	-0.02	99.88	65.40
13CH16	47°33'16.71"N, 121°17'51.91"E	47.74	2.20	12.80	11.75	0.16	11.21	9.35	3.08	1.62	0.42	-0.22	100.10	66.67
13CH17	47°33'05.93"N, 121°18'00.04"E	49.46	1.96	13.23	11.93	0.16	9.17	9.31	3.13	1.21	0.33	-0.42	99.47	61.71
13CH18	47°33'06.08"N, 121°17'59.67"E	49.77	1.94	12.96	12.10	0.16	9.19	9.52	3.27	1.24	0.37	-0.61	99.92	61.43
13CH19	47°33'05.81"N, 121°18'00.23"E	50.02	1.97	13.02	12.19	0.16	8.95	9.40	3.42	1.30	0.36	-0.62	100.18	60.62
14CH21	47°52'19.15"N, 121°12'33.72"E	49.18	2.18	12.51	12.44	0.17	10.04	8.80	2.99	1.60	0.49	-0.46	99.92	62.86
14CH22	47°52'47.61"N, 121°13'45.84"E	48.40	2.16	12.42	12.56	0.17	10.13	8.81	2.81	1.45	0.49	-0.06	99.34	62.84
14CH23	47°51'43.14"N, 121°16'18.85"E	49.28	2.25	13.16	12.33	0.16	8.49	9.27	3.10	1.42	0.45	-0.55	99.36	59.08
13TC01	47°21'52.88"N, 120°09'41.86"E	48.62	2.31	12.93	11.72	0.16	9.87	9.27	3.08	1.61	0.43	-0.10	99.90	63.85
13TC02	47°21'52.65"N, 120°09'41.71"E	48.95	2.22	12.90	11.93	0.16	10.07	9.15	3.23	1.59	0.39	-0.50	100.07	63.90
13TC05	47°17'15.04"N, 120°25'09.80"E	49.05	2.00	12.93	12.00	0.16	9.97	9.05	3.32	1.35	0.34	-0.59	99.58	63.53
13TC06	47°17'15.13"N, 120°25'10.03"E	48.74	2.04	12.87	12.17	0.16	9.98	8.90	3.45	1.35	0.36	-0.59	99.44	63.23
13TC07	47°18'09.05"N, 120°27'26.44"E	49.67	2.02	13.26	11.90	0.16	9.12	8.94	3.32	1.36	0.34	-0.60	99.49	61.64
13TC08	47°18'07.32"N, 120°28'03.52"E	47.94	2.19	13.19	11.47	0.16	9.75	9.06	3.55	1.81	0.49	-0.25	99.35	64.06

13TC09	47°19'59.78"N, 120°28'36.78"E	49.55	1.98	13.19	11.88	0.16	9.18	8.96	3.17	1.33	0.33	-0.57	99.17	61.84
13TC10	47°20'55.79"N, 120°28'50.65"E	48.47	2.09	12.68	12.30	0.16	10.34	8.81	3.20	1.46	0.39	-0.27	99.63	63.81
13TC11	47°20'55.90"N, 120°28'50.77"E	50.01	2.03	13.18	11.87	0.16	8.91	8.90	3.52	1.37	0.36	-0.48	99.83	61.15
13TC12	47°20'55.84"N, 120°28'50.51"E	48.40	2.04	12.44	12.18	0.16	10.71	8.84	3.40	1.45	0.38	-0.43	99.56	64.84
13TC13	47°22'17.46"N, 120°29'30.91"E	49.81	1.98	13.33	12.09	0.16	8.96	8.70	3.48	1.42	0.38	-0.45	99.88	60.85
13TC14	47°23'09.96"N, 120°29'23.99"E	50.32	1.99	13.45	11.64	0.16	8.93	8.89	3.40	1.30	0.33	-0.66	99.76	61.67
13TC15	47°22'21.13"N, 120°29'32.07"E	49.79	1.96	13.24	12.00	0.16	9.26	8.69	3.48	1.49	0.37	-0.51	99.94	61.81
13TC16	47°22'21.23"N, 120°29'31.88"E	50.53	1.92	13.53	11.43	0.15	8.85	8.90	3.18	1.24	0.35	-0.64	99.42	61.89
14TC21	47°18'06.82"N, 120°23'14.93"E	48.28	2.12	12.86	12.04	0.16	9.84	9.54	3.43	1.61	0.46	0.18	100.53	63.15
14TC22	47°17'20.42"N, 120°19'30.68"E	49.27	2.17	12.86	11.79	0.16	9.72	9.02	3.19	1.44	0.40	-0.57	99.43	63.35

注: 上标 a 表示  $Fe_2O_3^T$  (全铁) 以  $Fe_2O_3$  形式表示; 上标 b 表示假定  $Fe^{2+}/(Fe^{2+}+Fe^{3+})=0.9$ , 则  $Mg\# = 100 \times Mg^{2+}/(Mg^{2+}+Fe^{2+})$

附表 2 哈拉哈河-柴河玄武岩全岩微量元素( $10^{-6}$ )分析结果  
Appendix table 2 Whole rock trace elements ( $10^{-6}$ ) data for Halaha-Chaihe basalts

样品	BHVO-2																						
	13CH0	13CH0	13CHI	13TC0	13TC0	13TC0	13TC0	13TC1	13TC1	13TC1	13TC1	13TC1	14TC2	14TC2									
Li	7.90	7.58	7.35	7.65	7.88	7.31	7.35	7.82	8.40	4.64	4.50	7.24	8.37	8.32	8.10	8.39	8.08	8.48	8.56	8.04	8.25	7.96	8.02
Be	1.32	1.23	1.24	1.32	1.38	1.34	1.05	1.03	1.46	1.32	1.08	1.32	1.35	1.31	1.10	1.07	1.20	1.26	1.22	1.16	1.19	1.32	1.23
Sc	23.38	23.53	23.00	23.11	22.92	22.93	24.19	24.07	20.16	20.73	32.09	21.73	21.27	21.36	22.23	21.71	21.46	20.64	20.64	21.28	21.46	21.31	21.30
V	239.31	239.90	236.29	230.33	229.19	230.59	233.70	237.45	217.81	225.56	314.35	231.48	219.35	219.74	224.53	221.87	214.99	220.35	223.48	208.75	213.66	230.84	218.28
Cr	385.48	450.71	438.73	386.45	393.97	447.39	295.87	311.28	438.93	412.77	275.81	306.67	337.26	354.06	342.49	352.30	300.12	363.53	431.06	282.13	281.53	365.95	368.95
Co	55.01	56.21	55.58	52.42	52.91	53.85	50.85	51.32	53.34	54.45	45.34	50.17	50.51	51.27	53.40	53.65	51.22	54.50	57.55	50.65	51.66	52.93	53.46
Ni	291.44	331.13	331.13	279.95	289.24	310.71	249.42	255.21	283.19	309.35	120.85	174.23	251.19	270.82	285.81	293.69	240.58	321.47	362.13	232.41	232.85	262.81	301.04
Cu	117.44	136.49	133.37	116.66	117.98	119.06	117.61	97.49	103.87	100.60	129.21	87.94	110.69	126.57	103.92	91.12	128.06	140.21	126.27	122.71	116.75	118.26	160.62

Zn	113.23	107.24	108.42	114.19	109.36	108.97	107.56	110.57	112.24	126.45	122.56	102.20	104.00	119.89	115.21	115.66	117.70	119.19	116.99	121.54	122.01	117.31	118.66	116.20	115.86
Ga	18.47	18.03	18.09	18.54	18.64	18.69	18.50	18.34	18.53	18.89	18.49	21.27	21.40	19.10	19.33	18.97	18.94	19.01	19.25	19.24	19.37	19.63	19.92	18.47	18.47
Ge	1.36	1.36	1.33	1.38	1.35	1.37	1.36	1.36	1.28	1.39	1.42	1.60	1.62	1.43	1.33	1.32	1.37	1.38	1.38	1.36	1.42	1.41	1.44	1.38	1.39
Rb	31.25	28.48	31.66	31.56	32.25	31.72	29.40	23.34	24.49	29.23	26.33	9.48	9.26	20.83	29.57	32.07	25.13	24.35	27.57	28.09	28.50	24.62	25.49	31.85	29.00
Sr	488.95	497.75	644.33	487.25	489.03	527.77	503.78	356.21	360.15	521.49	488.70	403.98	394.00	493.49	555.95	462.51	415.86	408.86	396.67	430.22	392.80	390.45	474.02	428.25	
Y	24.64	23.05	22.98	23.27	23.82	23.79	23.19	23.06	23.10	26.03	25.74	26.61	25.90	24.25	23.58	23.35	22.50	22.80	22.76	24.42	23.53	21.79	21.90	23.93	22.84
Zr	166.80	154.22	159.51	166.71	174.01	175.76	171.97	136.05	138.43	163.90	155.09	172.65	171.00	147.91	177.22	167.07	145.12	145.68	147.38	157.55	154.01	146.51	147.09	156.39	161.73
Nb	52.88	46.04	47.77	49.24	49.82	50.37	49.81	37.80	38.95	48.09	44.48	18.94	18.10	39.79	51.40	48.89	42.05	41.96	45.28	47.09	45.82	42.13	42.23	52.63	44.53
Cs	0.45	0.39	0.42	0.41	0.44	0.47	0.40	0.16	0.14	0.35	0.19	0.13	0.10	0.14	0.30	0.27	0.12	0.15	0.34	0.38	0.38	0.26	0.28	0.33	0.26
Ba	424.83	381.49	401.25	428.79	458.18	469.77	472.62	344.49	349.37	345.15	345.93	131.13	131.00	328.43	487.82	434.74	387.01	365.08	355.31	365.23	340.75	331.59	338.50	426.79	390.48
La	25.59	22.60	23.78	25.00	25.41	26.01	25.34	19.50	19.92	25.11	23.35	15.71	15.20	20.13	26.58	24.90	21.89	21.77	21.69	23.84	22.35	19.49	19.84	24.52	21.85
Ce	49.00	43.76	45.90	47.73	48.21	49.06	47.77	36.96	37.72	51.78	47.97	37.61	37.50	41.68	49.73	47.05	41.32	41.53	40.69	46.29	44.43	38.37	38.55	48.11	43.56
Pr	5.97	5.26	5.52	5.75	5.79	5.90	5.73	4.46	4.54	6.63	6.25	5.26	5.34	5.44	6.00	5.64	4.97	5.04	4.86	5.53	5.38	4.60	4.67	5.97	5.48
Nd	25.39	22.48	23.60	24.30	24.53	24.92	24.35	19.17	19.42	27.03	25.61	24.84	24.30	22.80	25.64	24.10	21.22	21.59	20.70	23.51	22.69	19.79	20.03	24.18	22.66
Sm	5.84	5.30	5.45	5.56	5.65	5.72	5.66	4.74	4.76	6.25	6.00	6.17	6.02	5.61	6.00	5.62	5.10	5.21	5.04	5.55	5.17	4.68	4.71	5.70	5.45
Eu	1.94	1.78	1.81	1.86	1.87	1.91	1.89	1.61	1.62	2.00	1.92	2.08	2.04	1.83	2.01	1.92	1.75	1.78	1.72	1.88	1.80	1.64	1.69	1.86	1.79
Gd	5.73	5.21	5.30	5.43	5.56	5.55	5.55	4.88	4.91	6.14	5.87	6.16	6.21	5.63	5.89	5.60	5.23	5.34	5.19	5.70	5.38	4.89	4.95	5.72	5.46
Tb	0.84	0.77	0.79	0.80	0.81	0.81	0.80	0.74	0.74	0.91	0.89	0.93	0.94	0.85	0.83	0.82	0.77	0.78	0.78	0.84	0.81	0.73	0.74	0.85	0.81
Dy	4.70	4.40	4.41	4.47	4.51	4.58	4.50	4.27	4.31	5.06	4.93	5.35	5.28	4.66	4.57	4.55	4.39	4.45	4.37	4.74	4.55	4.15	4.23	4.69	4.52
Ho	0.85	0.80	0.80	0.81	0.82	0.82	0.82	0.80	0.81	0.89	0.87	0.99	0.99	0.84	0.82	0.80	0.79	0.81	0.80	0.85	0.81	0.74	0.76	0.83	0.78
Er	2.12	2.03	2.03	2.05	2.08	2.07	2.04	2.06	2.07	2.33	2.33	2.56	2.51	2.23	2.00	2.00	1.97	2.02	2.01	2.13	2.00	1.88	1.87	2.19	2.06
Tm	0.27	0.27	0.27	0.27	0.27	0.27	0.26	0.27	0.27	0.29	0.29	0.33	0.33	0.29	0.26	0.26	0.25	0.27	0.26	0.27	0.25	0.23	0.24	0.28	0.26
Yb	1.62	1.55	1.54	1.59	1.60	1.58	1.55	1.61	1.64	1.74	1.75	2.04	1.99	1.73	1.46	1.46	1.47	1.52	1.53	1.55	1.41	1.38	1.38	1.64	1.55
Lu	0.22	0.21	0.21	0.22	0.22	0.21	0.21	0.23	0.23	0.24	0.24	0.28	0.28	0.24	0.19	0.20	0.20	0.20	0.21	0.21	0.20	0.20	0.19	0.22	0.22
Hf	3.68	3.40	3.50	3.65	3.80	3.80	3.79	3.07	3.12	3.86	3.65	4.38	4.47	3.59	3.87	3.65	3.26	3.30	3.37	3.48	3.33	3.28	3.29	3.67	3.75
Ta	2.87	2.49	2.62	2.70	2.67	2.72	2.66	2.02	2.08	2.69	2.49	1.20	1.15	2.19	2.76	2.62	2.22	2.24	2.49	2.52	2.40	2.25	2.26	2.92	2.50
Pb	3.34	3.23	3.44	3.80	3.86	3.87	3.79	3.03	3.17	3.41	3.07	1.55	1.65	2.25	3.56	3.45	3.23	3.12	3.68	3.38	2.45	2.70	2.69	2.22	2.16

Th	3.50	3.08	3.25	3.55	3.65	3.69	3.58	2.73	2.80	3.99	3.47	1.25	1.22	2.77	3.73	3.47	2.99	2.88	3.26	3.16	3.15	3.05	3.06	3.55	3.18
U	0.86	0.72	0.68	0.92	0.81	0.86	0.77	0.60	0.58	1.18	0.98	0.42	0.41	0.72	0.70	0.66	0.43	0.51	0.76	0.81	0.76	0.66	0.59	0.85	0.75

注：上标 a 表明 BHVO-2 微量元素参考值据 Jochum *et al.* (2016)。

附表 3 哈拉哈河-柴河玄武岩全岩 Sr-Nd-Pb-Hf 同位素分析结果  
Appendix table 3 Whole rock Sr, Nd, Pb and Hf isotopes data for Halaha-Chaihe basalts

样品	$^{87}\text{Sr}/^{86}\text{Sr}$	ISD	$^{143}\text{Nd}/^{144}\text{Nd}$	ISD	$\epsilon_{\text{Nd}}^a$	$^{176}\text{Hf}/^{177}\text{Hf}$	ISD	$\epsilon_{\text{Hf}}^b$	$^{206}\text{Pb}/^{204}\text{Pb}$	ISD	$^{207}\text{Pb}/^{204}\text{Pb}$	ISD	$^{208}\text{Pb}/^{204}\text{Pb}$	ISD
13CH07	0.703 463	5	0.512 967	4	6.43	0.283 089	4	10.75	18.397 0	4	15.522 0	4	38.287 9	14
13CH08	0.703 613	6	0.512 974	4	6.55	0.283 099	7	11.09	18.388 1	5	15.517 4	5	38.267 3	15
13CH15	0.703 640	6	0.512 955	5	6.19	0.283 075	13	10.24	18.375 6	4	15.525 4	4	38.272 0	13
13CH16	0.703 586	6	0.512 965	4	6.38	0.283 079	10	10.38	18.366 9	5	15.521 1	5	38.260 8	11
13CH18	0.703 557	5	0.512 972	6	6.51	0.283 083	10	10.52	18.424 6	6	15.529 1	6	38.343 9	18
14CH21	0.703 748	3	0.512 906	8	5.23	0.283 087	11	10.67	18.529 7	5	15.538 4	5	38.354 3	17
14CH23	0.703 880	5	0.512 905	3	5.21	0.283 099	10	11.09	18.380 5	3	15.525 0	3	38.242 0	17
13TC01	0.703 787	4	0.512 913	5	5.37	0.283 068	9	10.00	18.376 3	5	15.519 6	4	38.318 9	19
13TC02	0.703 575	5	0.512 922	3	5.54				18.413 3	4	15.521 3	5	38.337 1	17
13TC07	0.703 569	3	0.512 945	4	5.98				18.474 0	5	15.542 3	5	38.333 7	21
13TC10	0.703 550	3	0.512 921	4	5.52	0.283 078	4	10.36	18.567 6	5	15.538 7	3	38.425 3	17
13TC12	0.703 577	3	0.512 942	4	5.93	0.283 087	7	10.68	18.508 6	4	15.543 1	5	38.372 5	13
13TC14	0.703 599	4	0.512 949	4	6.07	0.283 103	13	11.25	18.486 2	5	15.536 4	4	38.339 7	11
13TC16	0.703 589	3	0.512 930	7	5.69	0.283 099	11	11.11	18.479 1	4	15.538 3	5	38.335 6	18
14TC21	0.703 544	5	0.512 965	4	6.38	0.283 089	10	10.75	18.378 9	5	15.517 5	5	38.260 1	15

14TC22	0.703 609	3	0.512 938	4	5.86	0.283 070	9	10.08	18.418 8	4	15.524 4	3	38.325 2	16
BHVO-2 mean	0.703 466	8	0.513 017	3	7.55	0.283 107	4	11.39	18.634 5	10	15.486 4	8	38.171 0	22
BHVO-2 Ref. <sup>c</sup>	0.703 479		0.512 996		7.14	0.283 082		10.50	18.634 0		15.524 0		38.146 0	
BCR-2 mean	0.704 982	5	0.512 633	3	0.07	0.282 855	3	2.48	18.755 0	5	15.615 8	4	38.740 1	13
BCR-2 Ref. <sup>d</sup>	0.705 005		0.512 635		0.10	0.282 865		2.83	18.754 0		15.622 0		38.726 0	

注: 上标 a 表示  $\epsilon_{Nd} = [({}^{143}\text{Nd}/{}^{144}\text{Nd})_{\text{sample}}/({}^{143}\text{Nd}/{}^{144}\text{Nd})_{\text{CHUR}} - 1] \times 10^4$ ,  $({}^{143}\text{Nd}/{}^{144}\text{Nd})_{\text{CHUR}} = 0.512 630$  (Bouvier *et al.*, 2008); 上标 b 表示  $\epsilon_{Hf} = [({}^{176}\text{Hf}/{}^{177}\text{Hf})_{\text{sample}}/({}^{176}\text{Hf}/{}^{177}\text{Hf})_{\text{CHUR}} - 1] \times 10^4$ ,  $({}^{176}\text{Hf}/{}^{177}\text{Hf})_{\text{CHUR}} = 0.282 785$  (Bouvier *et al.*, 2008); 上标 c,d 表示 BHVO-2 和 BCR-2 放射成因同位素参考值据 Weis *et al.* (2006).

附表 4 以原始地幔为初始成分的批式部分熔融模拟计算参数

Appendix table 4 Parameters of trace element modeling of the batch partial melting of primitive mantle

$C^*$ (原始地幔)	D(Ol)	D(Cpx)	D(Opx)	D(Grt)	Ds	P	$C^L$ F=1%	$C^L$ (F=2%)	$C^L$ (F=3%)	$C^L$ (F=4%)
Rb	0.6	0.0004	0.01	0.0038	0.0003	0.00677	44.89	25.75	18.05	13.90
Ba	6.6	0.0011	0.00016	0.001	0.0002	0.000362	610.41	317.17	214.25	161.76
Th	0.0795	0.00005	0.006	0.0086	0.0008	0.003435	5.65	3.31	2.34	1.81
Nb	0.658	0.00007	0.0012	0.0007	0.001	0.000891	62.31	32.02	21.54	16.23
Ta	0.037	0.0002	0.0022	0.0008	0.0017	0.00169	3.40	1.77	1.20	0.91
La	0.648	0.0001	0.039	0.0006	0.0005	0.02732	36.40	23.54	17.39	13.79
Ce	1.675	0.0001	0.07	0.0017	0.0027	0.04913	68.93	49.55	38.67	31.71
Pr	0.254	0.0032	0.089	0.0083	0.0224	0.06326	8.00	6.17	5.03	4.24
Sr	19.9	0.00002	0.098	0.0021	0.0005	0.068446	671.13	510.69	412.16	345.50
Nd	1.25	0.0005	0.16	0.004	0.028	0.11455	28.19	23.50	20.15	17.63
Hf	0.283	0.004	0.215	0.017	0.11	0.05791	4.27	3.79	3.41	3.09

Sm	0.406	0.001	0.23	0.015	0.18	0.06395	0.1778	5.63	5.05	4.58	4.19
Ti	1.205	0.011	0.19	0.1	0.15	0.0859	0.1413	12753.08	11690.63	10791.59	10020.96
Tb	0.099	0.001	0.27	0.054	0.75	0.12472	0.2589	0.75	0.71	0.67	0.64
Ho	0.149	0.0031	0.25	0.1	2.6	0.26624	0.42593	0.55	0.54	0.53	0.52
Yb	0.441	0.05	0.22	0.22	4.92	0.481	0.639	0.91	0.90	0.90	0.89

注：a为源岩成分为原始地幔时某矿物初始比例，其矿物组成为Ol (40%)、Cpx (20%)、Opx (33%)和Grt (7%)；b为源岩成分为亏损地幔时某矿物初始比例，其矿物组成为Ol (62%)、Cpx (15%)、Opx (20%)和Grt (3%)；c为反应中熔体某矿物贡献比例，其矿物组成为Ol (30%)、Cpx (7%)、Opx (-10%)和Grt (10%)；F为固相部分熔融程度百分数；D<sup>o</sup>为初始固相和熔体相的总分配系数；P为进入熔体相中的固相和熔体相的总分配系数；C<sup>s</sup>为固相中某微量元素初始浓度；C<sup>l</sup>为固相熔融到熔体相中该微量元素浓度。原始地幔微量元素组成引自McDonough and Sun (1995)；亏损地幔微量元素组成引自Workman and Hart (2005)。Rb、Ba、Th、Nb、Ta、Sr、Hf、Ti和LREEs的分配系数引自Adam and Green (2006)；HREEs的分配系数引自Green *et al.* (2000)。